OPTIMAL DESIGN OF THE MAGNET PROFILE FOR A COMPACT QUADRUPOLE ON STORAGE RING AT THE CANADIAN SYNCHROTRON FACILITY

A Thesis Submitted to the College of Graduate and Postdoctoral Studies in Partial Fulfillment of the Requirements for the Degree of Master of Science in the Department of Mechanical Engineering, University of Saskatchewan, Saskatoon

By

MD Armin Islam

Permission to Use

In presenting this thesis in partial fulfillment of the requirements for a Postgraduate degree from the University of Saskatchewan, I agree that the Libraries of this University may make it freely available for inspection. I further agree that permission for copying of this thesis in any manner, in whole or in part, for scholarly purposes may be granted by the professors who supervised my thesis work or, in their absence, by the Head of the Department or the Dean of the College in which my thesis work was done. It is understood that any copying or publication or use of this thesis or parts thereof for financial gain shall not be allowed without my written permission. It is also understood that due recognition shall be given to me and to the University of Saskatchewan in any scholarly use which may be made of any material in my thesis.

Requests for permission to copy or to make other use of the material in this thesis in whole or part should be addressed to:

Dean

College of Graduate and Postdoctoral Studies

University of Saskatchewan

116 Thorvaldson Building, 110 Science Place

Saskatoon, Saskatchewan, S7N 5C9, Canada

Or

Head of the Department of Mechanical Engineering

College of Engineering

University of Saskatchewan

57 Campus Drive, Saskatoon, SK S7N 5A9, Canada

Abstract

This thesis concerns design of a quadrupole magnet for the next generation Canadian Light Source storage ring. The quality of the design is measured by the so-called width of Good Field Region (GFR) in the magnetic field generated by the magnet in a particular configuration, e.g. quadrupole configuration. The width of GFR is defined upon the multipole error in magnetic field strength, in particular the error being less than 0.1%. The design requirement for the magnet was to have the GFR at least ±1.0 cm. It is noted that the existing or preliminary design of the magnet (Dallin, 2018) has only achieved ±0.8 cm GFR. This thesis was motivated to design the magnet of the quadrupole so that the foregoing design requirement can be met. The secondary motivation of this thesis was to improve the design of the magnet so that the bad edge effect of the magnet can be reduced.

Increase of the width of GFR may be achieved by reduction of the multipole errors. The shape of the magnet pole is a major factor to cause these errors. An optimal design of the shape of the magnet pole was attempted in this thesis. Specifically, a simulation-based trial-and-error procedure was taken for the optimal design partly due to some difficulty to represent the shape of the magnet pole analytically. This procedure was acceptable as a pilot try for a more sophisticated optimal design that may follow in the future. Reduction of the bad edge effect with the magnet may be reduced by careful modification of the shape of the side or edge of the magnet.

The result of this thesis is very encouraging; specifically, the width of ±1.1 cm of GFR has been achieved within the field region. The result thus gives a proof of the proposed design approach with the procedure. Further, the bad edge effect was also reduced.

This thesis has made a contribution in the field of synchrotron radiation machinery with the proposed design approach to the magnet. The proposed approach is simple and can be implemented in any synchrotron radiation facility.

Acknowledgements

First, I would like to express my sincere gratefulness to my supervisors Dr. Chris Zhang and Dr. Mark Boland for their constant support. Their incredible guidance and motivation helped me to successfully complete my MSc study program. Starting from the coursework, giving me a summer internship at Canadian Light Source Inc., helping me with the research proposal, guiding me through the whole research and writing the thesis, I can't think a better supervisor than them. Also, their guidance and contribution to my attending to a conference as well as conference paper writing, opened a new door of my expertise for which I will always be grateful to them. I would also like to thank my advisory committee members, Dr. Daniel Chen and Dr. Madan M. Gupta, for their helpful advice and suggestions from the first Advisory Committee meeting.

I would also like to express my gratitude to Les Dallin who is an accelerator physicist and scientist at Canadian Light Source Inc. for his extended collaboration and valuable suggestions which contributed greatly to the development of this research. Also, I would like to thank Drew Bertwistle who is also an accelerator physicist at Canadian Light Source Inc. for providing me the necessary software licenses and the software using instructions. Again, a special thank goes to the Canadian Light Source staff especially Accelerator Operations and Development (AOD) staff, for their help and co-operation without which it would be difficult to accomplish the goal of this research.

Finally, I would like to express my profound gratitude to my parents and my siblings for providing me continuous encouragement and support throughout my whole study program. This accomplishment would not have been possible without their support.

Table of Contents

List of Figures

List of Tables

List of Abbreviations

CLS	Canadian Light Source
GFR	Good Field Region
ESRF	European Synchrotron Radiation Facility
SIS	Schwer Ionen Synchrotron
RCS	Rapid Cycling Synchrotron
J-PARC	Japan Proton Accelerator Research Complex

Chapter 1 : Introduction

1.1 Background of the Research

A synchrotron radiation facility creates electromagnetic radiation of different wavelengths by circulating high energy electrons in an orbit. The storage ring is comprised of different kinds of electromagnets including dipoles, quadrupoles, and sextupoles. The name of a magnet depends on the number of magnetic poles that it contains. For example, a dipole magnet has two poles, a quadrupole magnet has four poles, a sextupole magnet has six poles, and so on. Dipole magnets bend the electron beam and keep the beam constrained to a roughly circular path. When the electrons are deflected by dipole magnets, they emit synchrotron radiation over a wide range of different wavelengths. Quadrupole magnets focus the beam and keep the beam constrained to near the orbit defined by the dipoles. Stronger focusing results in a brighter source of radiation. Sextupole magnets control the focusing of off-momentum particles. This thesis concerns the design of a compact quadrupole magnet.

A novel quadrupole has been designed for use in a possible new storage ring for the Canadian Light Source (CLS 2.0) (Dallin, 2018). This quadrupole is novel because of some of its unique features. There are only two coils required for this quadrupole magnet as shown in Figure 1.1. For a conventional quadrupole usually four coils are required. The coils are recessed into the outer yokes as shown in Figure 1.2. As such, that the coil does not stick out beyond the yoke. This allows a reduction of the drift space between magnet elements. The drift space is the physical space between magnets placed side by side in the synchrotron latticed as shown in Figure 1.3. It is noted that the coils in this quadrupole occupy none of the drift (owing to the recessed structure of the coil with respect to the yoke). This design is referred to as a Zero Drift Quadrupole.

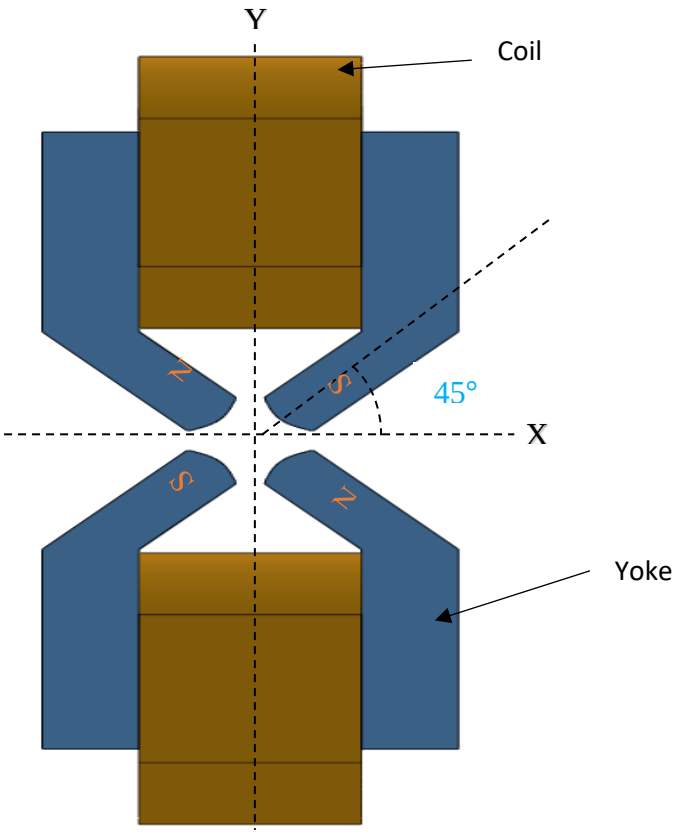

Figure 1.1: Model of the quadrupole showing its two north poles and two south poles.

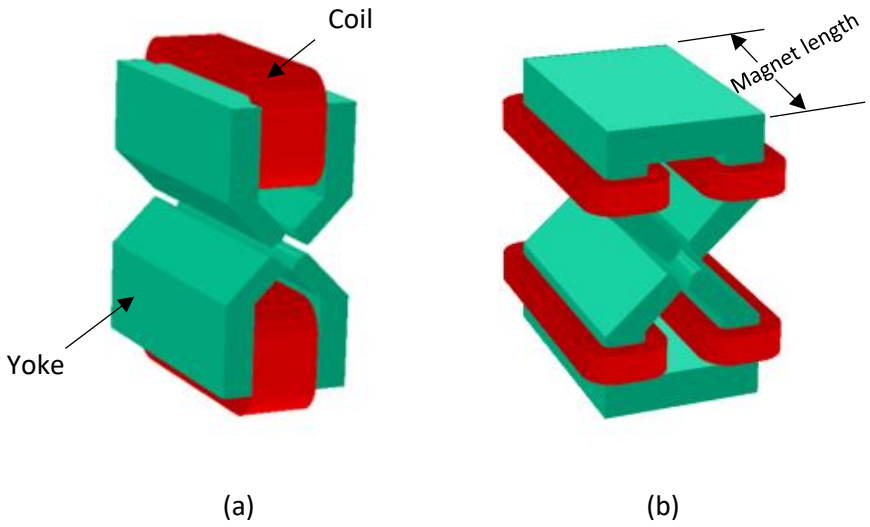

Figure 1.2: (a) Zero Drift Quadrupole (Coil does not stick out beyond the magnet length), and (b) Conventional Quadrupole (Coil sticks out beyond the magnet length)

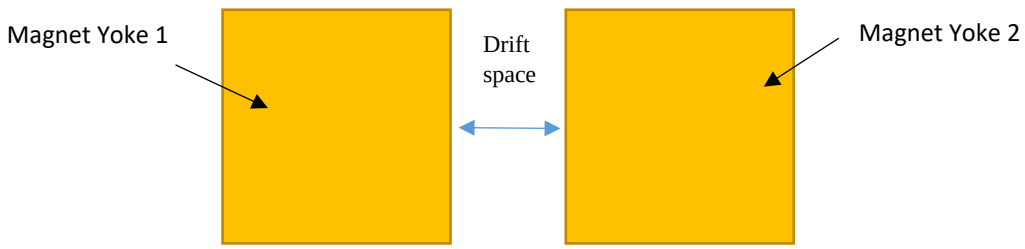

Figure 1.3: Drift Space between two magnets. (More space is required if the coils stick out beyond the yoke.)

The shape of the magnet pole is responsible for the magnetic flux and the quality of the magnetic field (see Figure 1.4). The ideal pole shape of quadrupole is an infinite hyperbola. However, in practice, there is always a cut-off point which gives a finite hyperbolic curve (see Figure 1.5). According to the existing magnetic design, the ideal hyperbola was cut to truncate the pole at the points of x=5.76 cm, y=4.41 cm and y=5.76 cm, x=4.41 cm (see Figure 1.5).

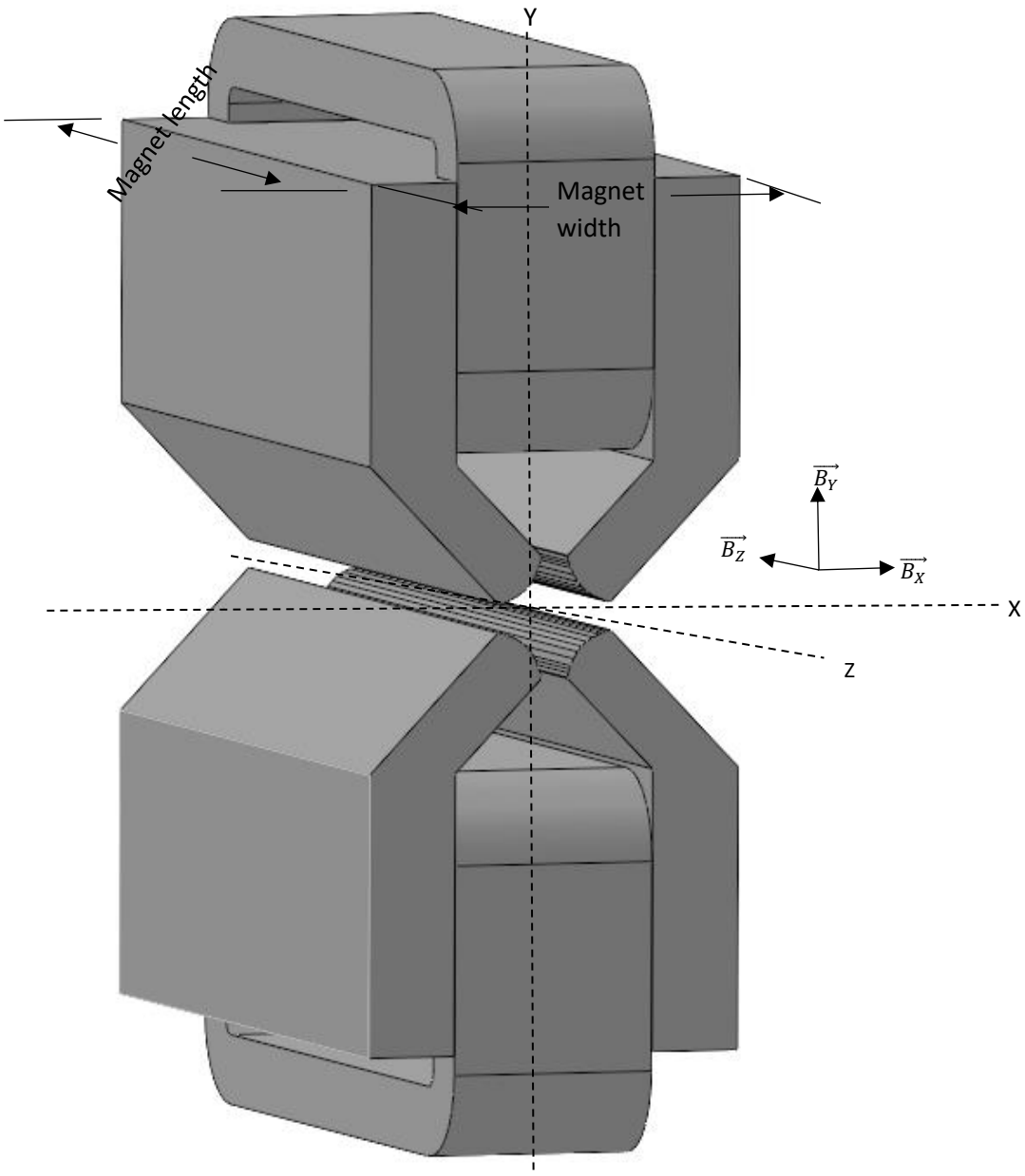

Figure 1.4: Perspective 3D model of the quadrupole showing the magnetic fields ($\overrightarrow{B_X}, \overrightarrow{B_Y}, \overrightarrow{B_Z}$).

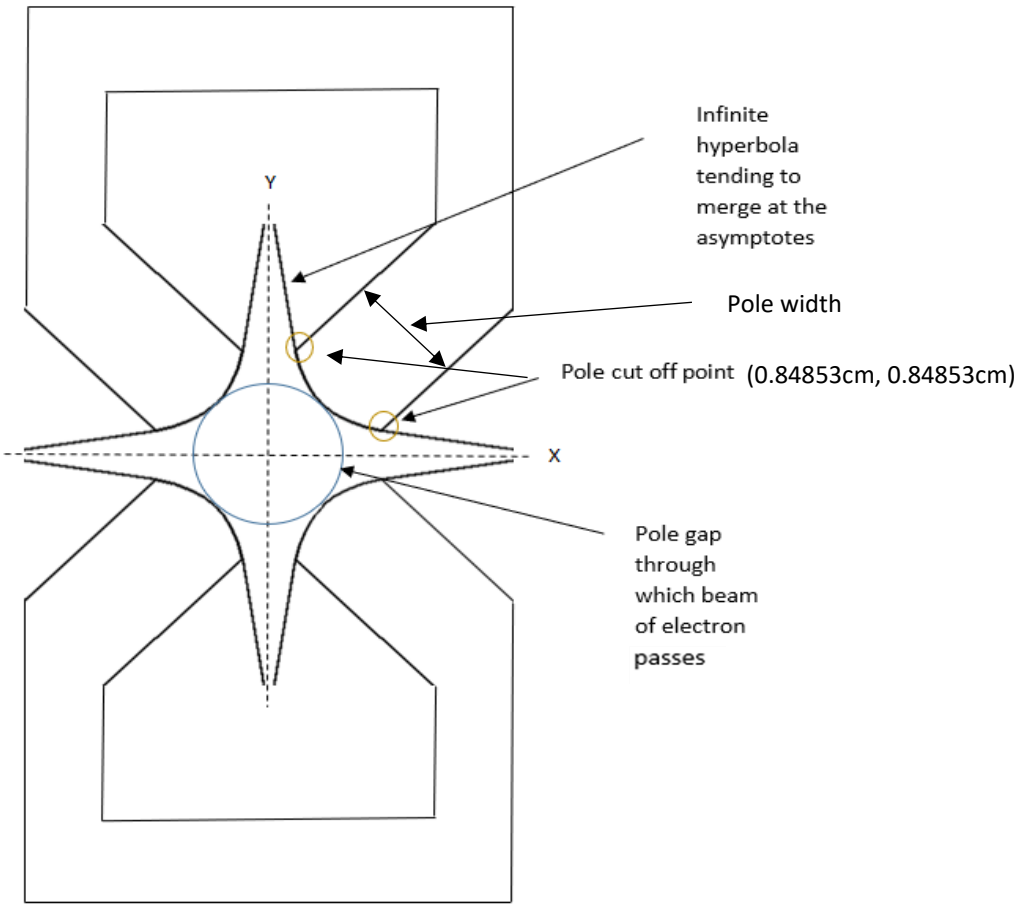

Figure 1.5: Front view of the quadrupole yoke. An infinite hyperbola is cut at certain points (yellow circles) to make the pole which is fourfold axisymmetric.

As stated above, the purpose of the quadrupole magnet is to focus the electron beam. The magnetic field of the quadrupole is zero at the center of the magnet and increases linearly with the distance from the center (see Figure 1.6). Depending on the polarity of the current in the coils the quadrupole can be focusing or defocusing. A focusing quadrupole focuses the electron beam horizontally and defocuses vertically. On the other hand, the defocusing quadrupole defocuses horizontally and focuses vertically.

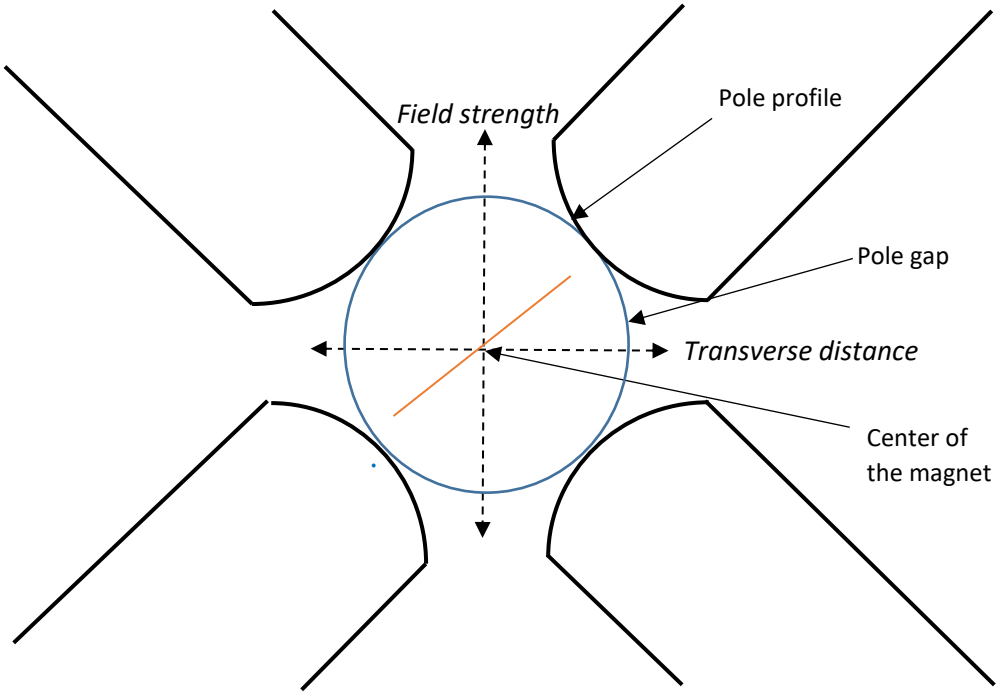

Figure 1.6: Field ($\vec{B}$) distribution of a quadrupole electromagnet, which increases linearly with the transverse distance from the center of the magnet.

1.2 Motivation and Research Problem

A magnet has two or more poles called a multipole magnet. A quadrupole is a multipole magnet. The magnetic field potential of a particular multipole magnet is a sum of the field potentials of all different magnets. The magnetic potential (B) at any point (x, y) in a multipole magnet is expressed by the Fourier expansion as

$$B(x,y) = \sum_0^\infty B_n(x+iy) = B_0 + B_1(x+iy) + B_2(x+iy)^2 + B_3(x+iy)^3 + \cdots \quad \ldots\ldots (1.1)$$

where, B's are the potentials of different magnets. A pure quadrupole field contains only the $(x+iy)^2$ term. By decomposing the $(x+iy)^2$ term (Tanabe, 2005), the pole profile of a pure quadrupole found is expressed by

xy= Constant. ……..…. (1.2)

This means that the shape or profile of a quadrupole magnet is an infinite hyperbola. It is noted that on the magnet there will be coils around it. As such, the infinite hyperbola magnet is not practical, and in fact, in practice, the magnet has a finite width (see Figure 1.5, pole width in particular). The magnet with a finite width will then create higher-order (greater than 2) harmonics, which is called multipole errors. The magnetic potential of a practical quadrupole is then expressed by

$$B(x,y) = B_2(x+iy)^2 + B_6(x+iy)^6 + B_{10}(x+iy)^{10} + B_{14}(x+iy)^{14} + \cdots\cdots \quad \ldots. (1.3)$$

where, B_2 is the amplitude of the quadrupole field strength. To a four-fold axis-symmetric configuration of magnets (see Figure 1.6), only B_6, B_{10}, B_{14}, ... harmonic amplitudes are presented, which are called **errors in a quadrupole**. These errors significantly affect the quality of the quadrupole field and in particular, they reduce the width of the good field region (GFR) which is defined as the region from the center of the magnetic field (Figure 1.6) such that these errors are less than 0.1% of the desired good field region.

There is another problem with the finite width of the magnet. Along the Z-axis (see Figure 1.4) or called longitudinal direction, in the field close to the two edges of the magnet, the field line may become curved out (Figure 1.7a). Ideally, the design of the magnet should ensure the field line as straight as possible (Figure 1.7b) and the multipole error is as small as possible, ideally less than 0.1%.

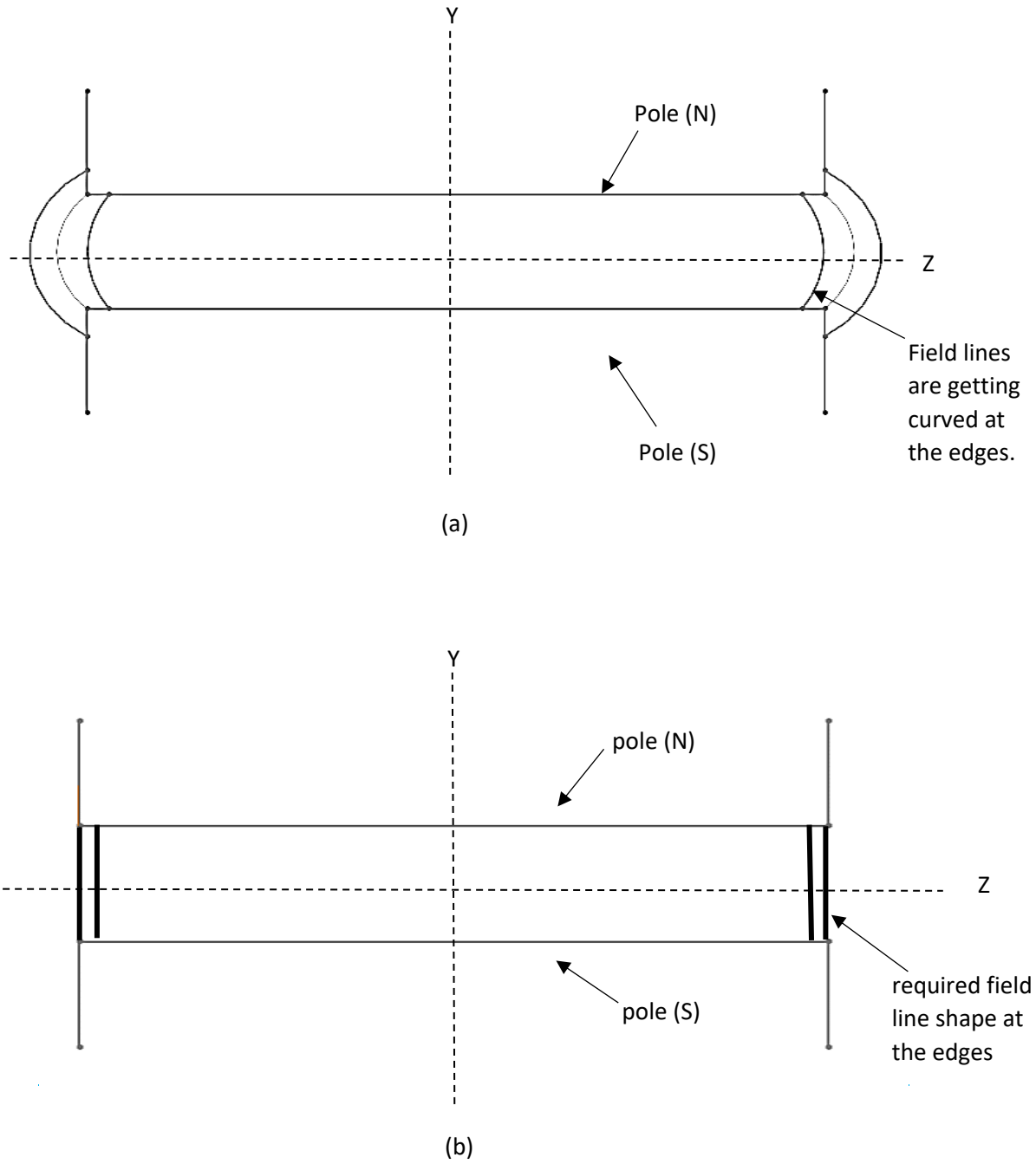

Figure 1.7: Field line shape of (a) existing design, (b) required design at the edges.

This thesis was motivated to improve the existing design of the profile of pole of quadruple magnets so that the width of GFR can be increased from ±0.8 cm of GFR to ±1.0 cm of GFR at least and the field line around the side of the magnet is as straight as possible.

1.3 Research Objectives and Scope

The **overall objective** of this thesis research was to improve the quality of the magnetic field for the quadrupole magnet, including the increase of the width of GFR (to make it greater than ±1.0 cm from the center of the field) and reduction of the edge effect of the magnet. The following specific objectives were defined to facilitate the research:

- ***Objective 1****: To propose a new design concept for the profile of the pole of a quadrupole magnet so as to increase the width of GFR to be as much as possible (at least greater than* ±1.0 cm from the center of the magnetic field).

It is noted that an existing magnetic design of the quadrupole for the next generation storage ring of Canadian Light Source (CLS 2.0) was conducted by Les Dallin at CLS (Dallin, 2018). To this design, the magnet length is 24 cm and the required magnetic field gradient for the quadrupole was above 50 T/m. This magnetic design was built by following the law of electromagnetism (Ampere's law) and is with a compact shape (see Figure 1.2). The compactness in shape can facilitate the close placement of the quadrupoles in the storage ring. The existing design of the quadrupole has achieved the magnetic field gradient of 54.06 T/m. The shortcoming with this design is that the width of GFR is ±0.8 cm, which is short of the required width of GFR, that is, ±1.0 cm. This thesis research was expected to improve this design. The design was further under the following constraints:

- Pole gap cannot be less than 2.4 cm (see Figure 1.5).
- Pole width is fixed (1.91 cm) (see Figure 1.5).

- ***Objective 2:*** *To propose a new design concept to the magnet, especially the profile of the edge of the magnet so that the bad edge effect with the magnet can be reduced as much as possible.*

The edge effect[1] was explained before (see Figure 1.7). In the existing design (Dallin, 2018), the edge effect was left for further research.

On a general note, the methodology to carry out the proposed research was based on a simulation and trial-and-error procedure to seek an optimal design. A rigorous algorithmic procedure was not taken given the size of the problem and difficulty of having some analytical equations available.

1.4 Organization of the Thesis

The remaining part of this thesis is organized as follows. Chapter 2 will provide further background information and literature analysis of some related work pertinent to the proposed research objectives. This chapter also discusses the existing magnetic design of the quadrupole. In Chapter 3, the magnetic field in a quadrupole will be illustrated comprehensively along with the concept of multipole error and good field region. The purpose of the discussion is to build a foundation for the reader to understand the simulation system used in this thesis, which is able to find the potential of the magnetic field and calculate high order harmonics (i.e., multipole errors). The simulation system will be a tool for design evaluation. Chapter 4 will discuss the improved design of the profile of the pole of the magnet and the improved design of the edge of the pole by using the simulation system discussed in Chapter 3. Chapter 5 concludes this thesis.

[1] It is noted that in the literature, sometimes, the term 'end effect' is used. In this thesis, the edge effect and end effect are interchangeable.

Chapter 2 : Background and Literature Review

2.1 Introduction

The purpose of this chapter is to give further background information and literature pertinent to the proposed research objectives in Chapter 1. Section 2.2 will discuss about the different electromagnets that the synchrotron facility uses. In Section 2.3, the requirement for quadrupole design will be discussed. Section 2.4 will discuss some of the optimizations of the pole shape that other synchrotrons performed in the design of the quadrupole electromagnet and then will try to critically comment on those optimizations. Section 2.5 will discuss an existing design of the quadrupole magnet at CLS.

2.2 Electromagnets in a Synchrotron

An electromagnet is a magnet that produces a variable magnetic field using electric current, so it consists of wires that are wound into coils which are further mounted on the magnet. To the magnet in synchrotron facility, the coil is placed around a yoke made from the ferromagnetic or ferromagnetic material. The coil carries a current that creates a magnetic field concentrated in the coils. The magnetic core concentrates the generated magnetic flux and the shape of the magnetic core gives the shape of the field. There are usually three kinds of electromagnets used in a synchrotron facility: dipoles, quadrupoles, and sextupoles.

2.2.1 Dipole

A dipole magnet has two poles: one North (N) and one South (S) (see Figure 2.4), creating a field that is 90^{o} with respect to the horizontal axis as shown in Figure 2.1. According to the right-hand convention rule, if the coil current is flowing in the indicated direction shown in Figure 2.1, the magnetic flux flows downward, and the N is positive while S is negative. Such dipole magnets provide horizontal bending to the electron beam. The dipoles define the reference orbit for the electrons. Using the right-hand convention, for a positive beam current into the page, force direction is to the left.

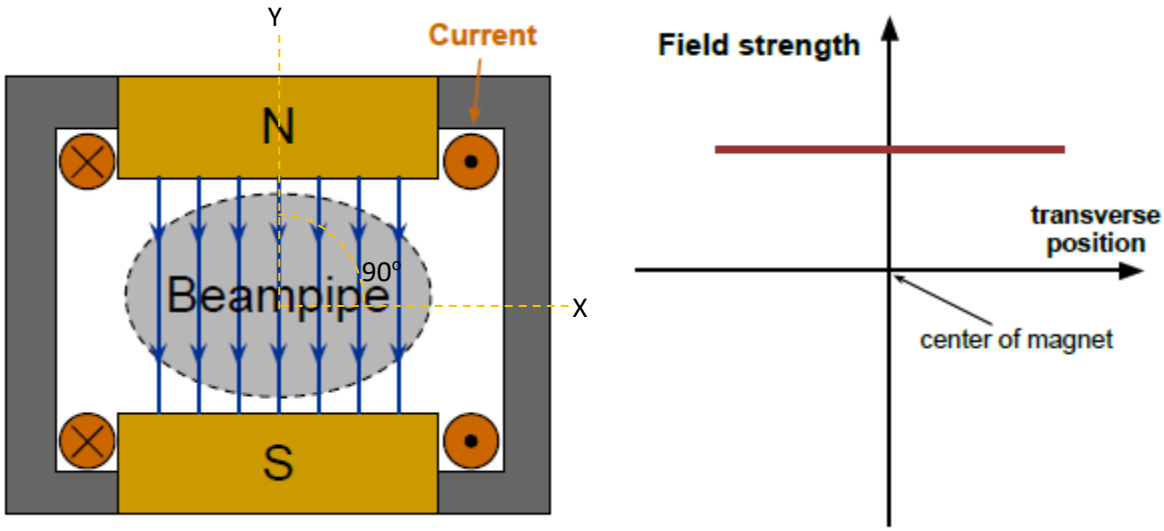

Figure 2.1: Schematic 2D model of a dipole and its field distribution (Fermilab, 2013).

2.2.2 Quadrupole

A quadrupole magnet has four poles: two norths and two souths. In a standard configuration, each pole is at an angle of 45^{o} with respect to the horizontal and vertical axis as shown in Figure 1.1. According to the right-hand convention rule, if the coil current is flowing in the direction shown in Figure 2.2, the magnetic flux will flow outward from the poles at $\pi/4$ and $5\pi/4$ and inwards to poles at $3\pi/4$ and $7\pi/4$. A quadrupole magnet provides transverse focusing to the particle and keeps the beam constrained within the beam pipe. The field strength of a quadrupole is zero at the center of the magnet and increases linearly with transverse displacement as shown in Figure 2.2. An arrangement of quadrupoles in a lattice is made in such a way that the quadrupoles can oscillate off-axis electrons transversely around the center of the beam pipe.

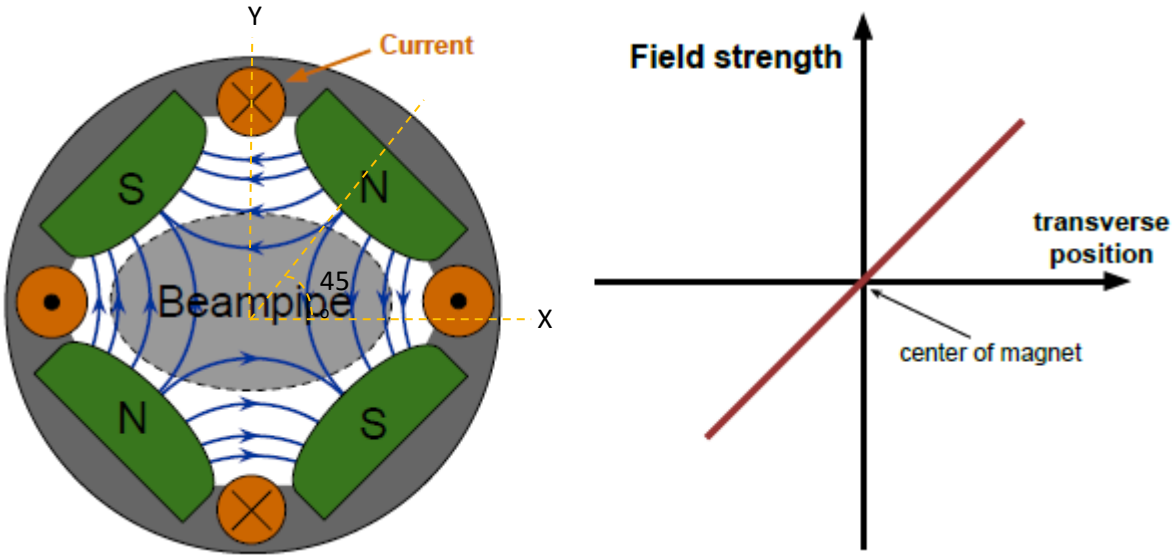

Figure 2.2: Schematic 2D model of a Quadrupole and its field distribution (Fermilab, 2013).

2.2.3 Sextupole

A sextupole magnet has six poles and a zero-field at its center as shown in Figure 2.3. The field is normal to the horizontal centerline and centerlines at angles $\pi/3$ and $2\pi/3$. The field distribution of a sextupole magnet is quadratic. The field strength varies with the square of the displacement from the center of the magnet. The main purpose of a sextupole is to correct chromatic aberrations arising from electrons being off momentum. Such particles will be incorrectly focused in the quadrupoles.

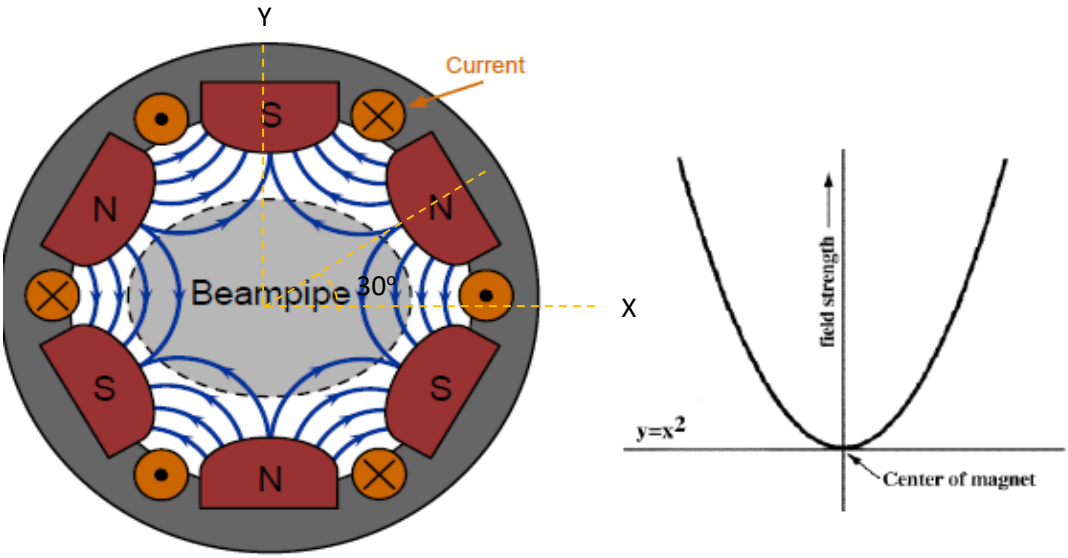

Figure 2.3: Schematic 2D model of a sextupole and its field distribution (Fermilab, 2013).

2.3 Requirements for the Quadrupole

In this section, the overall requirements to build a quadrupole electromagnet will be discussed, as this thesis is focused on design of the quadrupole electromagnet or magnet. There are basically two kinds of requirements to build a quadrupole.

(1) Magnetic requirements of the quadrupole.

(2) Structural requirements of the quadrupole.

2.3.1 Magnetic requirements of the quadrupole

The magnetic requirements are the first concern while making an electromagnet. As stated earlier, the magnetic field of the quadrupole increases linearly in the transverse direction (XY plane) from the center of the beam. The components of the magnetic field ($\vec{B}$) for an ideal quadrupole in the X-Y plane transverse to the beam are thus:

$\vec{B}_y = k\,x$ ..... (2.1)

Similarly,

$\vec{B}_x = k\;y$ ..... (2.2)

In the above equations, k specifies the field gradient, x is the horizontal displacement from the center, and y is the vertical displacement from the center. The sign of k determines whether the quadrupole will focus or defocus the particles in the horizontal plane.

The force exerted on the electron beam by a quadrupole magnetic field can be described by the Lorentz Force. The Lorentz force on a particle of charge q and velocity v due to electric field E and magnetic field B is,

$$\vec{F} = q(\vec{E} + \vec{v} \times \vec{B}) \quad \text{.....(2.3)}$$

The direction of the Lorentz Force and magnetic flux in a quadrupole is shown in Figure 2.4. Consequently, the force is proportional to the displacement from the quadrupole center.

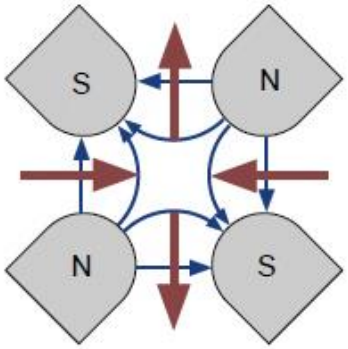

Figure 2.4: The blue arrows show the direction of the magnetic flux while the red arrows indicate the direction of the Lorentz force on a positive particle going into the image plane (Fermilab, 2013).

2.3.2 Structural requirements of the quadrupole

The basic structural components of a quadrupole electromagnet are the yoke and coil. Yokes are made of ferromagnetic or ferrimagnetic materials. The shape of the magnetic field depends on the shape of the yoke. The strength of the magnetic field highly depends on the permeability of the yoke material. The magnetic permeability of a material defines the ability to hold the development of a magnetic field within itself. While choosing the material, there are some other attributes that

are considered such as saturation, coercivity, remanence, resistivity and lamination thickness, and so on.

An electromagnetic coil is a current conductor. The coils are basically a wire that wound around the yoke. The wires are usually made of copper because of its high electrical conductivity. This wire wraps around the yoke of the magnet by a determined number of turns. In a coil, the wire must be insulated with a nonconductive insulation coating to avoid the current from passing between the wire turns. The ends of the wire are attached to an external circuit. In an electromagnetic coil, there is an inside hole in the wire to facilitate the cooling fluid flow to control the temperature due to current flow through the coil, so as to avoid the effect of temperature on the beam stability.

The magnetic field of an electromagnet is proportional to the number of turns of wire in the coil, (N) and the current in the wire, (I) and hence the product, NI (ampere-turns) which is called magnetomotive force. The magnetic field path (Path1 + Path2 + Path3 + Path4 + Path5) in a quadrupole is shown in Figure 2.5. The length L_{yoke} (Path 2 + Path 3 + Path 4) of this magnetic field path is in the yoke material and the length L_{gap} (Path 1+ Path 5) is in the air gaps. Now according to Ampere's Law, we can get the following:

$$NI = H_{yoke}L_{yoke} + H_{air}L_{air} \quad \text{..... (2.4)}$$

$$NI = B\left(\frac{L_{yoke}}{\mu} + \frac{L_{air}}{\mu_0}\right) \quad \text{..... (2.5)}$$

where μ =B/H is the magnetic permeability of the core material at the particular B field used. H is the field strength. $\mu_0 = 4\pi\ (10^{-7})$N. A^{-2}, is the permeability of free space (or air). Equation 2.5 is a nonlinear equation because the permeability of the yoke (μ) varies with the magnetic field (B).

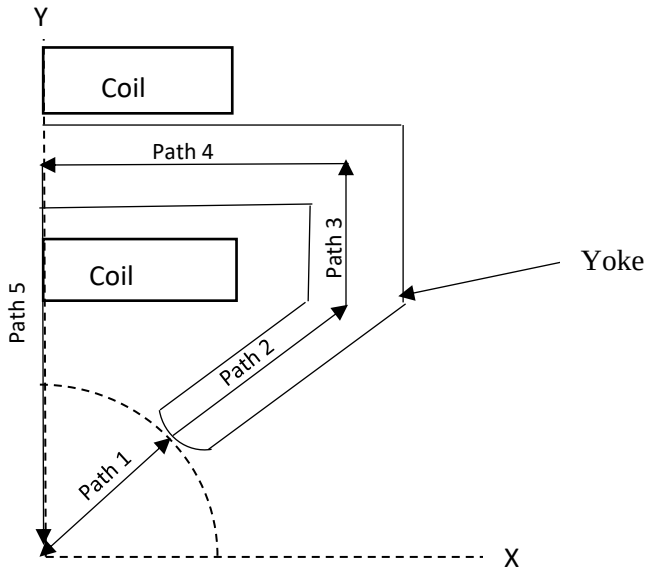

Figure 2.5: Magnetic field path in a quadrupole.

Coils can be placed at different positions on the yoke according to the requirement of the design, as shown in Figure 2.6. For example, in a conventional shape quadrupole, the coils are placed around the side part of the yoke (see Figure 2.6a). The quadrupole which was studied in this thesis has coils wounded around the top part of the yoke (see Figure 2.6b). Also, the number of coils changes with the placement of the coil on the yoke. A conventional shape quadrupole needs four coils (Figure 2.6a), while the quadrupole studied in this thesis has two coils only (Figure 2.6b).

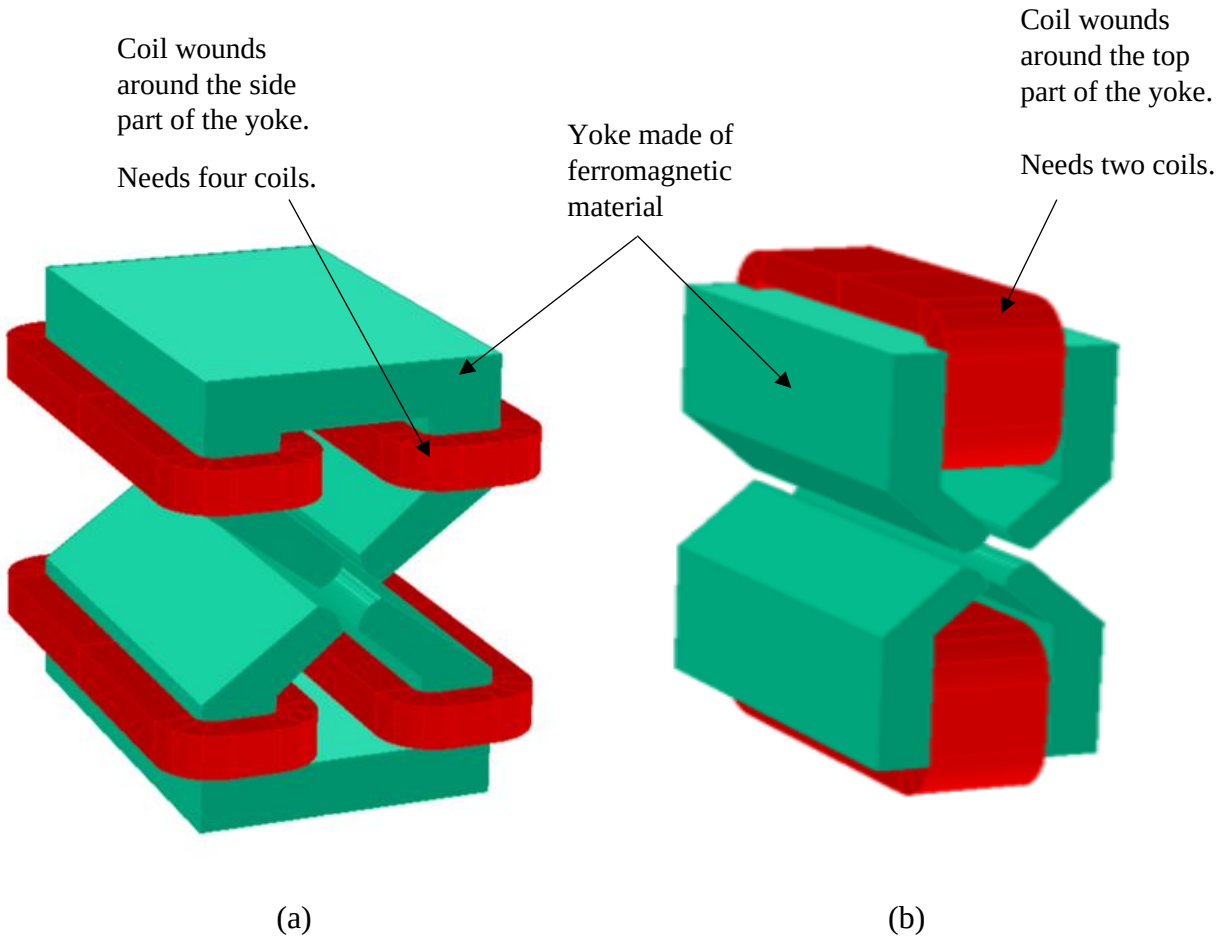

Figure 2.6: (a) 3D model of a conventional shape quadrupole using four coils on the side part of the yoke, (b) 3D model of the quadrupole using two coils that are recessed into the top of the yoke (zero-drift quadrupole).

2.4 Design of the Pole Shape of the Quadrupole in Different Synchrotrons

Various synchrotron facilities have been working on the optimal design of the pole shape for their magnets. One example of pole shape design is the ESRF II quadrupole pole (Le Bec et al., 2014). The European Synchrotron Radiation Facility (ESRF) is a combined research synchrotron facility situated in Grenoble, France, and is the strongest source of synchrotron in regards of generated light, producing X-rays which 100 billion times brighter than the X-rays used in hospitals (ESRF, 2019). The facility is now being updated to the next-generation synchrotron facility (ESRF II) with

a new design of the quadruple magnet. The conditions of the magnet for the ESRF II lattice are high gradients, bigger good field region, and large vertical gaps. An attempt was made to optimize the pole shape of the ESRF II quadrupoles to achieve the desired performance of the magnetic field. The decision variable for the optimization was the shape of the pole. The objective function was the higher-order harmonics and the optimization problem is to determine the pole shape so that the high-order harmonics are minimized. The constraint of this optimization problem was related to the restriction on the pole gap. The minimum pole gap considered was 11 mm with the magnet length 500 mm and material low carbon steel, AISI 1006. The nominal gradient for quadrupole was determined to be 90 T/m. The optimization problem was a non-linear problem. The Radia magnet simulation software (Chubar, 1998, Elleaume, 1997) was used for field computation. The variation in the field for a particular point does not scale with the variation of the pole shape harmonics. An instinctive method called Gauss-Newtonian algorithm (Nocedal, 1999) was used to optimize the problem. The algorithm converges in less than 10 iterations.

After the optimization, a very low relative harmonics amplitude was found, resulting in a 7 mm GFR (the field error 0.1%). The end effects (multipole errors at the end of the magnet) of the magnet have also been corrected within this pole profile (see Figure 2.7) (Le Bec et al., 2014). But following the method, the desired amounts of the field gradient at the middle area along the length of the magnet (Z-axis, see Figure 1.4) and at the end of the magnet, respectively, have not been achieved, because the nature of their design is to optimize the pole shape for the harmonics in the transverse direction (in the X-Y plane, see Figure 1. 4). This design does not meet the requirement at CLS, which this thesis considered, i.e., the width of GFR being at least $\pm$10 mm or $\pm$1.0 cm.

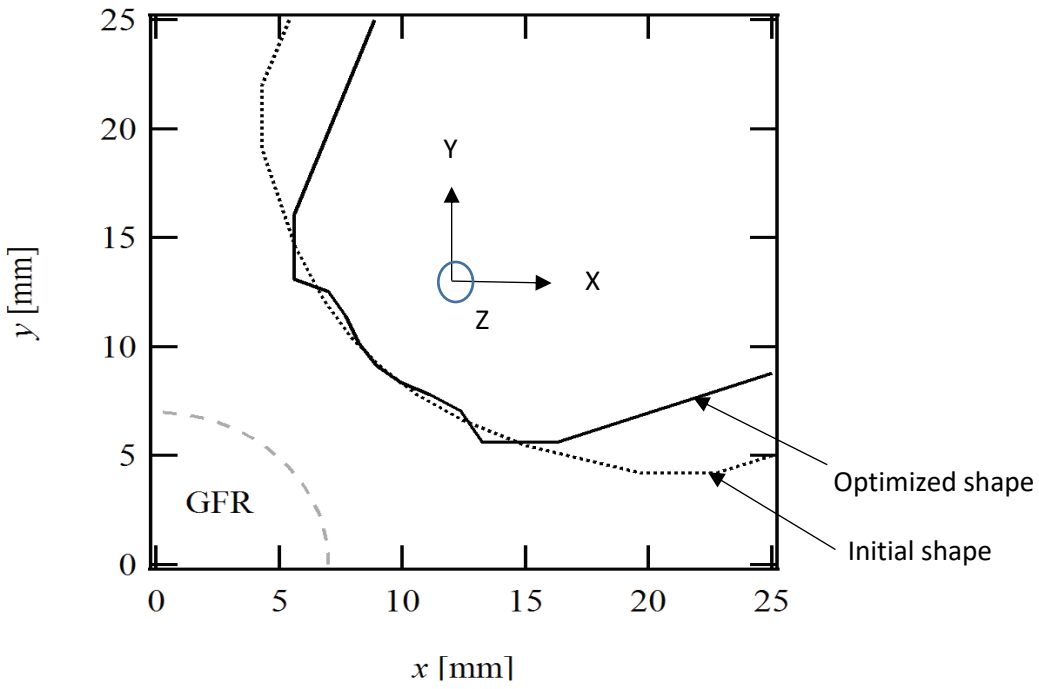

Figure 2.7: Dotted line: initial pole shape, 8 mm gap between poles; Solid line: Optimized pole shape, 11 mm gap between poles, dashed line: Good Field Region (Le Bec et al., 2014).

Another attempt for optimizing the pole shape for a quadrupole was performed at SIS-100 (Schwer Ionen Synchrotron, or heavy ion synchrotron) (Kalimov et al., 2006). The SIS-100 is a charge particle accelerator and situated in Darmstadt, Germany. It was founded as a part of the project, Facility for Anti-proton and Ion Research (FAIR). The SIS-100 is equipped with magnets containing superconducting coils and iron yokes. The idea of the optimal design with their magnets is to compensate for the higher-order field harmonics by deforming the pole profile. The optimization variable was the shape of the pole and the constraint functions were the pole width and pole gap. The objective function was the higher-order harmonics (i.e., B's as shown in the discussion of Chapter 1), which are denoted by 6, 10… 22. The pole profile was described in terms of Fourier series corresponding to the field expansion for the infinitely wide pole and further considering the pole profile as a line with the constant magnetic potential, and they got the following equation:

$U(r,\theta) = \sum_{j=1}^{J} P_j \;.(r/g)^j\,.\cos(j.\theta) = const.$ ……………………………..……. (2.6)

The parameters Pj defines the amplitude of the harmonics on the pole surface, g is the pole gap radius and r, θ defined polar coordinate for each point on the pole profile. It is noted that here P stands for B (discussed in Chapter 1), and the polar coordinate system is used here instead of the Cartesian coordinate system. The optimization process was first to define the pole profile as a constant magnetic potential line which has a constant value. This constant value is the summation of the magnetic potential for all considered field harmonics absolute value. The field harmonics were assumed as the harmonics on the pole surface. The constant value was supplied in Equation 2.4 from the existing design. After that, the required amplitudes of each field harmonics which were assumed as the harmonics on the pole surface were supplied in Equation 2.4. Then for different values of θ's, the values of r's were found which (θ, r) gave the new pole profile (see Figure 2.8). The optimization procedure for the quadrupole magnets was integrated into the software ***MULTIMAG,*** for computing magnetic fields in accelerator magnets (Kalimov et al., 2006). One drawback of this technique is the assumption that the amplitudes of the harmonics are identical of those within the pole gap and those on the pole surface. This assumption may introduce a significant error, as the amplitudes are not constant in the field within the pole gap.

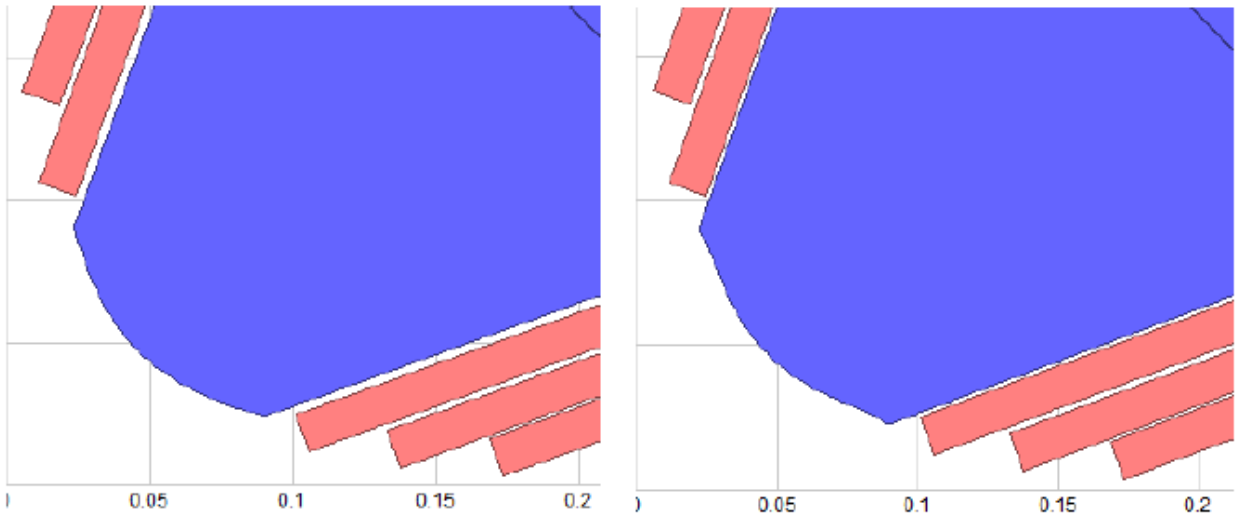

(a) (b)

Figure 2.8: (a) Cross-section of the pole profile before, and (b) after optimization (Kalimov et al., 2006).

Yet, another example of pole shape optimization is J-PARC quadrupole optimization. The rapid cycling synchrotron (RCS) of the Japan Proton Accelerator Research Complex (J-PARC), 3-GeV synchrotron facility is a high-power pulsed proton driver. Seven correction quadrupole magnets were built for this synchrotron facility. Measurement of the magnetic field showed that the magnetic field requirements were not met. The necessity of improving the design of the magnet to achieve the required performance became mandatory. Optimization of the pole shape was performed in OPERA-3d/TOSCA to retain the required magnetic field performance of the quadrupoles (Tani et al., 2016). The decision variable in the optimization model was the shape of the pole and the constraint function was the pole gap. The objective functions were the allowed higher-order harmonics. The optimal design was performed by attaching additional pole pieces (steel plate) (see Figure 2.9) on the pole. Different sizes for the plate were examined for achieving the required performance[2]. As a result of this optimal design, the required performance was achieved. A prototype was made, as shown in Figure 2.10, where the additional pieces are glued

[2] Note that optimal design or design optimization in this thesis is much broader than the mathematical definition of an optimization problem; especially the solving process may not be any kind of algorithmic procedure but perhaps an educational trial-and-error procedure.

to the pole profile, and the clearance between the two is about 0.5 to 1 mm (Tani et. al, 2016). The shortcoming with this approach lies in the assembly of these additional pieces on the pole profile, including the radiation effect on the glue and being prone to mechanical error.

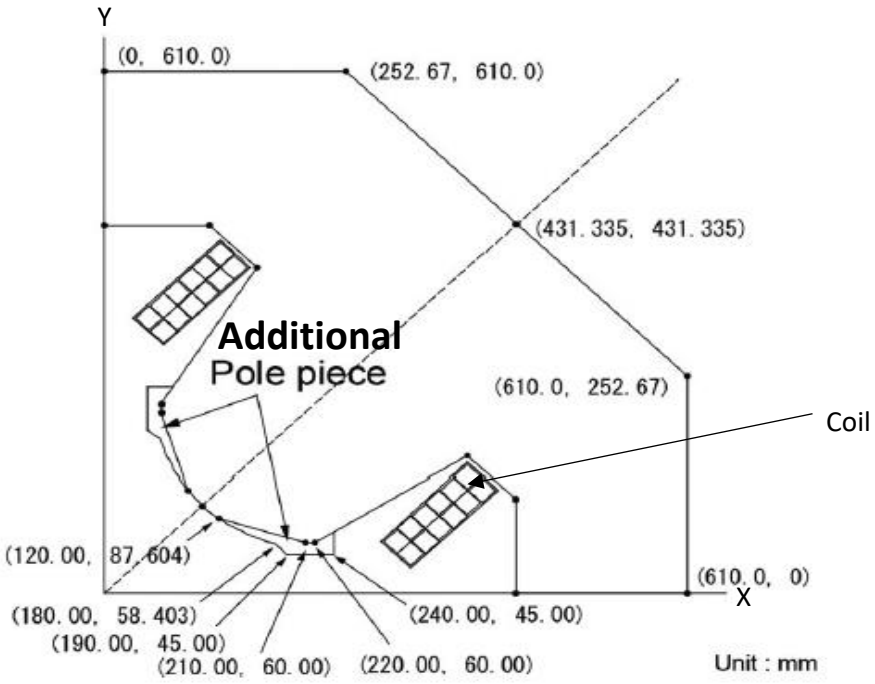

Figure 2.9: Quarter-sectional drawing for the pole shape of the optimized quadrupole (Tani et al, 2016).

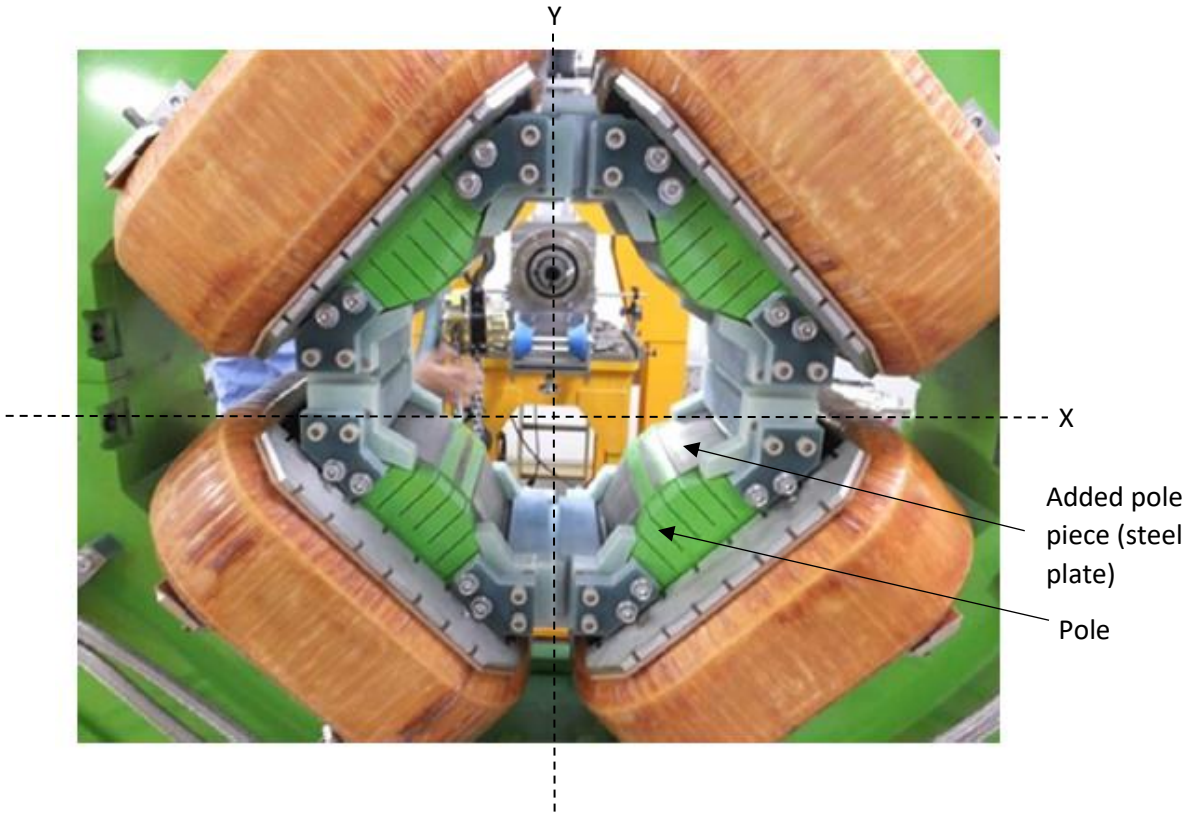

Figure 2.10: Overall view of the pole pieces installed in the quadrupole poles (Tani et al, 2016).

2.5 Existing Magnetic Design of the Quadrupole at CLS

At CLS, a concept design of a quadrupole was developed, which consists of two yokes with each having a coil. One of the salient points with this concept design is that the coils are recessed (see Figure 1.2), so the design is compact. The pole profile is circular with the radius of 1.2 cm in order to achieve the field gradient of larger than 50 T/m or 5000 G/cm. The magnet length is 24 cm, and the current in the coils is 4020 Amp-turns (per coil). Figure 2.11 shows the 3D drawing model of the quadrupole as well as the pole shape.

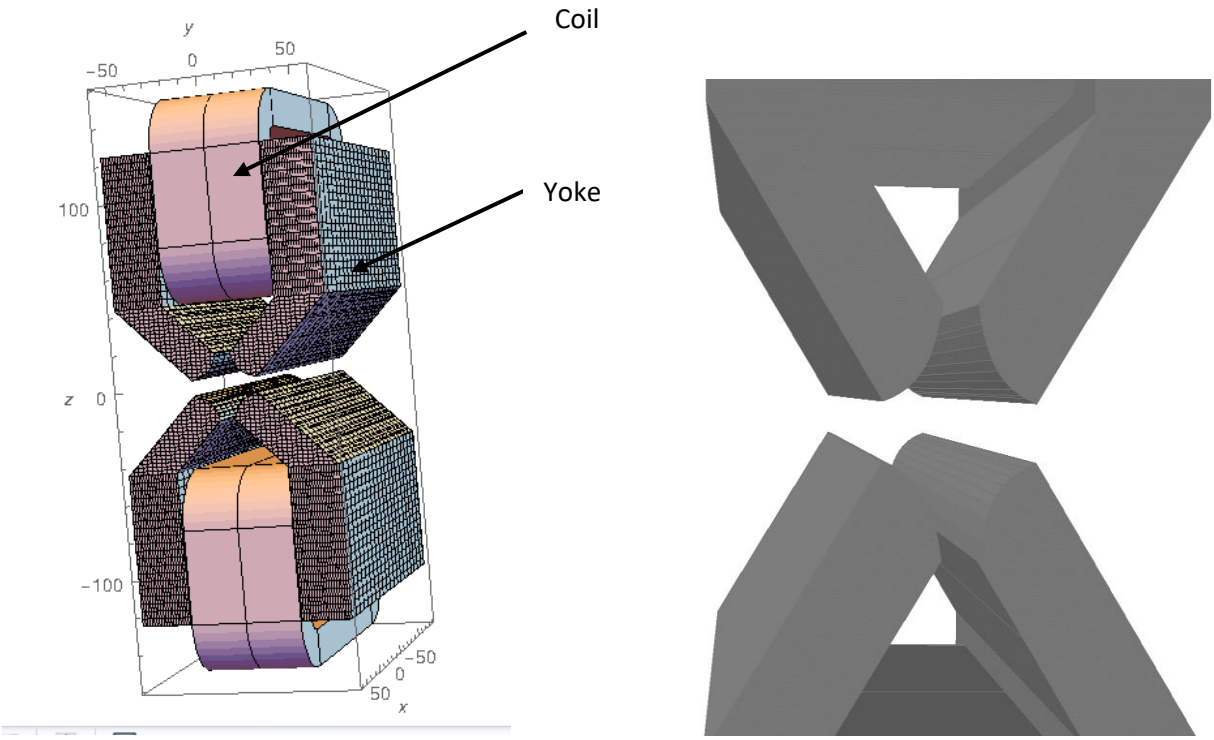

(a) (b)

Figure 2.11: (a) Existing magnetic model structure of the quadrupole, (b) Existing 3D pole shape (Dallin, 2018).

The 2D magnet code POISSON software was used to simulate the field quality of this design**.** Multipole errors were calculated in a circle of radius 1.0 cm inside the pole gap, and the result is shown in Figure 2.12. The design achieved the quadrupole gradient of 54.06 T/m or 5406 G/cm and good field region found of 1.6 cm ($\pm$0.8 cm) (the total multipole error of 0.1%). Figure 2.13 shows the magnetic field in the field region. It can be seen from the figure that beyond the good field region (total multipole error is less than 0.1%), the error is quite large. Clearly, this design can only achieve the GFR of $\pm$0.8 cm.

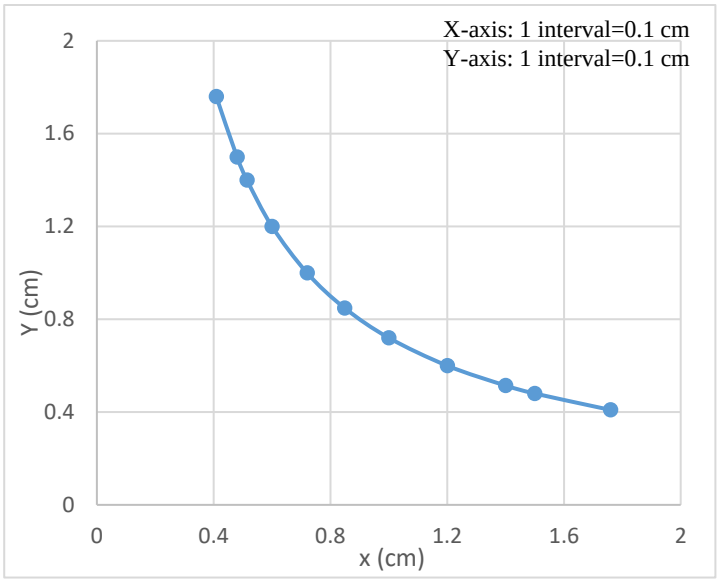

2	5.4060E+03
6	-8.8408E+00
10	-2.0988E+00
14	-1.0726E+00
18	6.4977E-02
22	1.9474E-01
26	3.5001E-01

(a) (b)

*Figure 2.12:***(**a) Existing pole shape, (b) Existing multipole errors (Field coefficient of the multipole errors are in Gauss and distance is in cm) (Dallin, 2018).

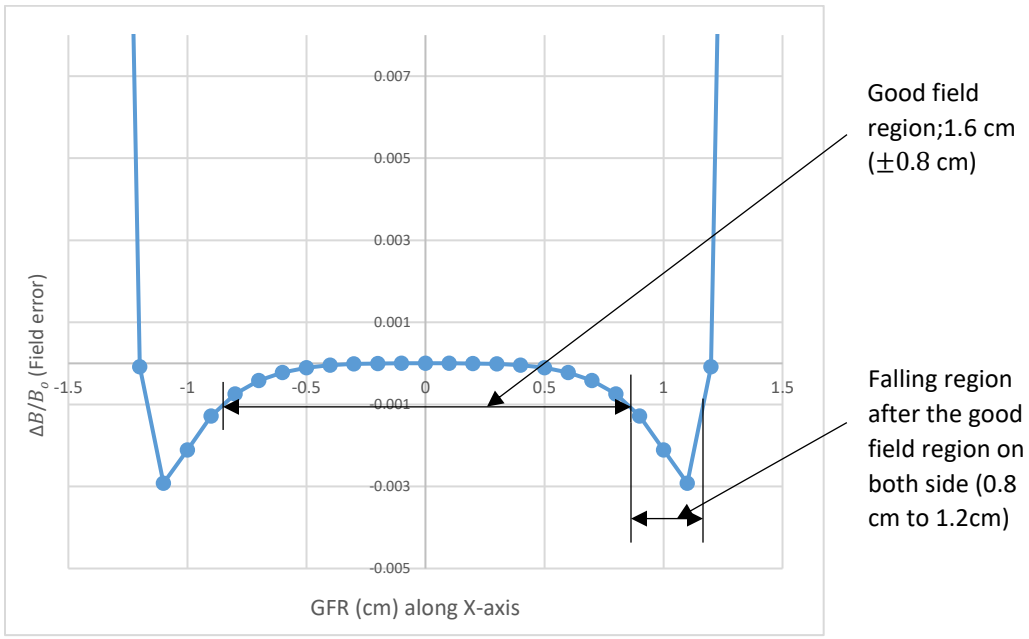

Figure 2.13: GFR of the existing quadrupole design.

The effect of the design feature of recessed coil in terms of the field profile along the Z-axis was examined using the 3D simulation software called RADIA (Chubar, 1998, Elleaume, 1997). Figure 2.14 shows the result of this simulation. It can be seen from this figure that the magnetic field is constant over the whole magnet length along Z-axis (offset, x=1.0 cm). This magnetic field distribution of the quadrupole has been compared with the magnetic field distribution of a similar configuration conventional shape quadrupole. It was found out from the comparison that recessing the coil has no effect on the field distribution of the magnet over the whole magnet length. The amplitude of the harmonics at the edges of the magnet was calculated using OPERA (OperaFEA, 2019). Specifically, the software calculated the multipole errors from 3 to 18 inside a circle of 1.0 cm radius at the edge along the pole gap (see Figure 2.14b). The amplitudes are shown in Table 2.1. From this table it can be seen that the multipole errors had the amplitude enough that made the field lines curved at the edges (see Figure 1.7a).

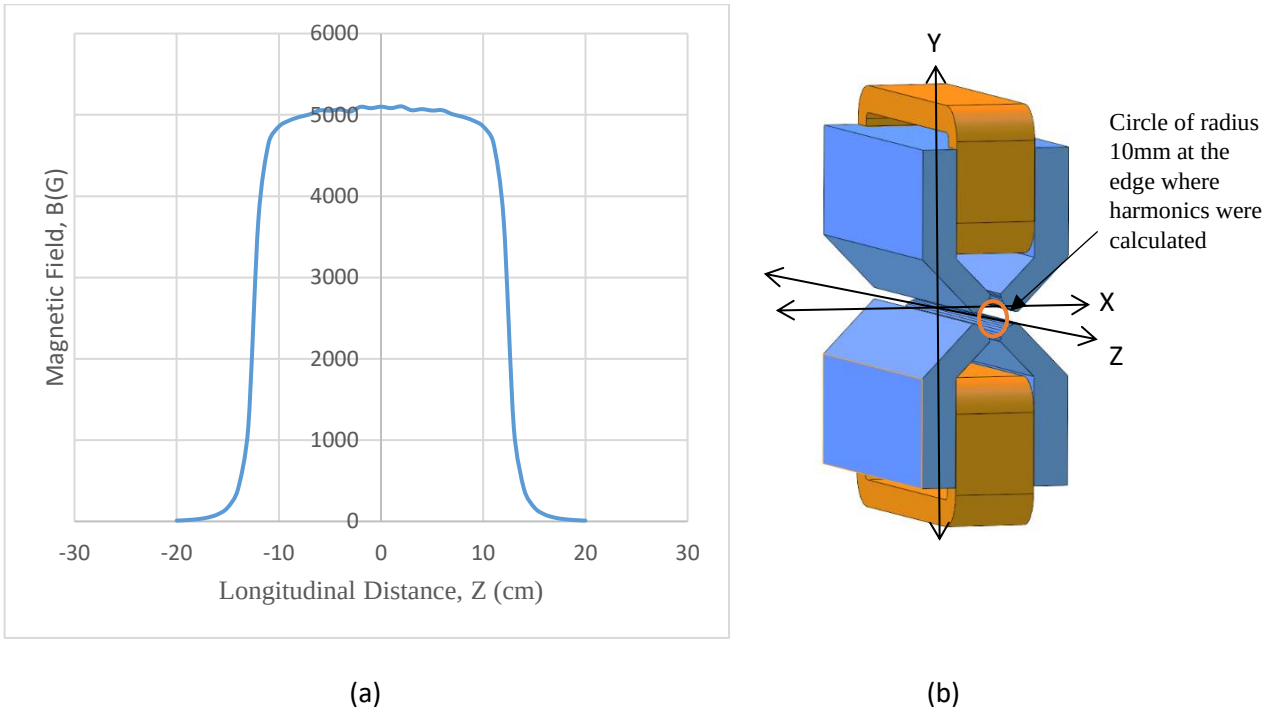

Figure 2.14: (a) Field distribution along the Z-axis, inside the pole gap and X=1.0 cm offset, (b) perspective model of the quadrupole to show the direction of the field distribution.

Table 2.1: Multipole errors at the edges. Field coefficient of the multipole errors are in Gauss (G) and distance is in cm.

Multipole error	Existing model
B_3	4.08
B_4	-2.17
B_5	1.44
B_6	-67.8
B_7	-1.44
B_8	-3.94
B_9	-8.00
B_{10}	6.32
B_{11}	2.86
B_{12}	-1.03
B_{13}	-2.40
B_{14}	0.927
B_{15}	-1.79
B_{16}	-1.34
B_{17}	-1.77
B_{18}	1.87

2.6 Conclusion

The pole cut off point leaves an important effect on the field quality of the quadrupole magnet. To achieve the required field quality, the pole shape is an important factor. Different optimal design strategies for the pole shape were taken at different synchrotron facilities worldwide. These optimal strategies have pros and cons. At the time this thesis study was conducted, it was decided that a new optimal design strategy should be taken not only because a new concept design is available to this study but also none of the existing ones is convincing to this new concept design.

Chapter 3 : Analysis of the Quadrupole

3.1 Introduction

This chapter will discuss the magnetic field generated from the quadrupole magnet, especially the relationship of the pole shape or profile of the magnet and the multipole errors. This relationship is a foundation to discuss the optimal design of the pole shape, so the width of the good field region (GFR) is greater than ±1.0 cm (the multipole errors < 0.1%). In Section 3.2, the process of generating a magnetic field from a quadrupole electromagnet will be described. In Section 3.3, the concept of multipole errors or higher-order harmonics in a quadrupole will be discussed. In Section 3.4, the good field region (GFR) in a quadrupole will be discussed. In Section 3.5, the governing equation for the magnetic field is introduced, which is the foundation of the simulation system discussed in Section 3.6. Section 3.7 is a summary.

3.2 Magnetic Field in a Quadrupole

All the electromagnets are built on the principle of Ampere's law, which is known as the law of electromagnetism. Ampere's Law says that the magnetic field created by an electric current around an arbitrarily shaped conductor is equal to the vector sum of the magnetic field created by the current around each segment of the conductor (Opentextbc.ca, 2019). According to this law, a current passing through a wire generates a magnetic field that curls around the wire (see Figure 3.1) and by winding many turns on a coil, a strong uniform magnetic field can be created (see Figure 3.2).

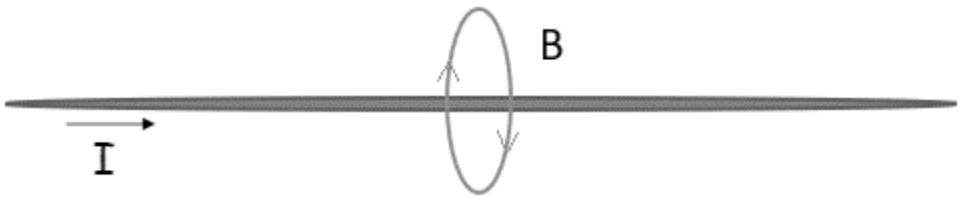

Figure 3.1: Process of generating a magnetic field ($\vec{B}$) by passing an electric current (I) through a wire.

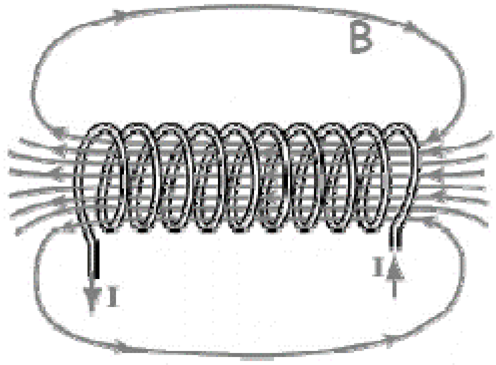

Figure 3.2: More winding creates a stronger magnetic field (Holmes et al. 2009).

The field strength is given by one of the Maxwell's equations (Tanabe, 2005):

$$\vec{\nabla} \times \vec{B} = \mu\mu_0 J \quad \text{……………………………………………………………} (3.1)$$

where,

- $\vec{\nabla}$ = Curl; is a vector operator.
- $\vec{B}$= Magnetic flux density (T).
- μ= Permeability of magnet material (N/A^2).
- μ_0= Permeability in air (N/A^2).
- J= current density (A/m^2).

Following the law of electromagnetism, the current-carrying wires are wrapped around the four metal cores to create a quadrupole magnet (see Figure 2.2 and Figure 2.4). The field lines are denser near the profile of the pole which means the field is stronger there. As stated in Equation 2.1 and 2.2, the strength of B_y is a function of x and vice-versa.

As stated before, quadrupole magnets focus and defocus this beam. An array of quadrupoles can keep the beam constrained to a region around the reference orbit. The focusing and defocusing characteristics of a quadrupole magnet are analogous to focusing and defocusing characteristics of

optic lenses. According to the optical analogy of a lens (see Figure 3.3), focusing a ray of light at the focal point is expressed by f. The deflection angle depends on the distance from the center, x. The farther offset from the principal axis, the stronger the deflection effect.

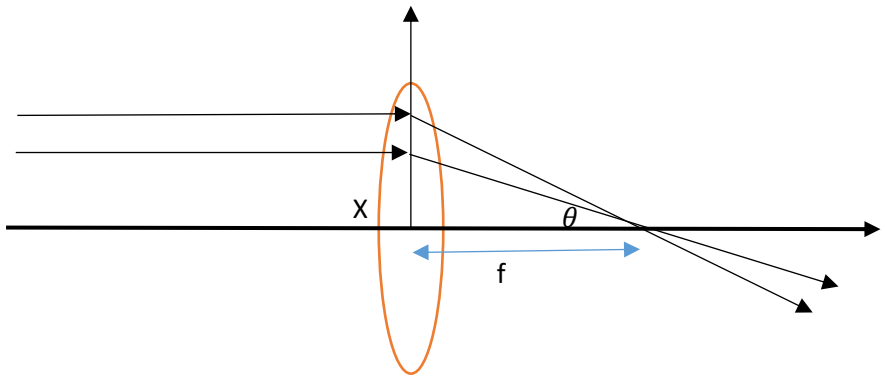

Figure 3.3: Optical analogy of a lens which is completely analogous for a quadrupole focusing characteristics.

Like the optical lens, the quadrupole provides a transverse focusing on the particle beam that is offset from the center of the magnet. Since the magnetic field increases linearly with *x*, the resulting focusing will also increase linearly with x.

The focusing direction of the quadrupole on a positive particle (see Figure 3.4) can be illustrated following the conventional right-hand rule. If a positive particle is going into the page then according to the right-hand rule, the Lorentz force (see Chapter 2, Section 2.3.1) on the particle of the upper side of the magnet is upward, and the force on the particle of the lower side of the magnet is downward. The force on the particles of the right and left sides will be toward the center. This magnet will horizontally focus and vertically defocus the particles. Swapping the polarity of the magnet pole, the focusing and defusing directions will be swapped.

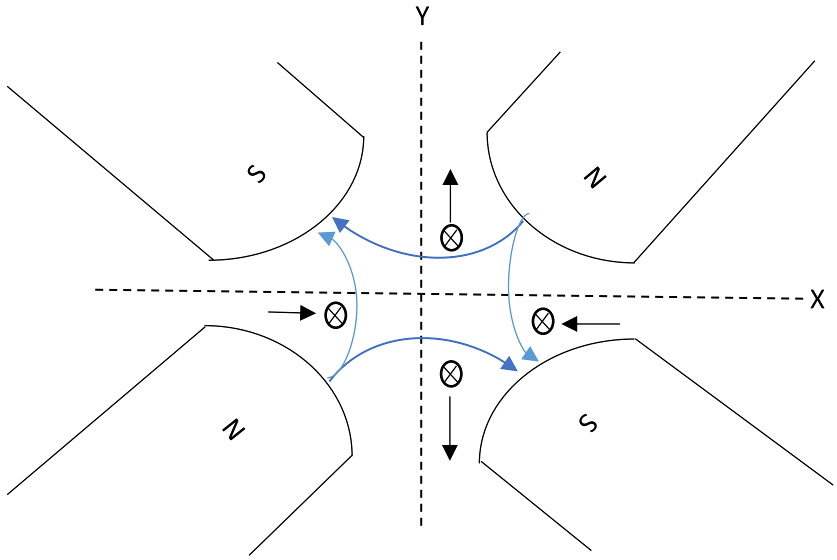

Figure 3.4: The curved blue arrows showing the direction of the magnetic flux**.** The black arrows showing the direction of Lorentz force.

3.3 Multipole Errors in a Quadrupole

As stated earlier, a multipole magnet has two or more poles such as dipole, quadrupole, sextupole, octupole and so on. In the electromagnetic analysis, the multipole is used to define the harmonic content of the field. Thus, a dipole magnet can have errors which consist of harmonics called multipole errors. Similarly, a quadrupole magnet can have multipole errors. The multipole errors arise in an electromagnet due to pole design and fabrication error. An electromagnet is actually characterized by a spectrum of these harmonics. Magnetic Fields are conventionally characterized by the complex function (Tanabe, 2005).

$$F = B_N Z^N + \sum_{n \neq N} B_n Z^n \quad \text{……………………………………………………………} (3.2)$$

where F is a complex function that represents the magnetic field of a multipole magnet. N is the index of the desired magnet field; B is the field potential and Z=$x + iy$ is a complex number on the XY plane. The $\sum_{n \neq N} B_n Z^n$ term represents the spectrum of higher-order harmonics of the

magnet, which are called the multipole errors. For N=2 in Equation 3.2, the complex function of the magnetic field of a quadrupole can be found, which is

$$F = B_2 Z^2 + \sum_{n \neq N} B_n Z^n$$

$$F = B_2 (x + iy)^2 + \sum_{n \neq N} B_n (x + iy)^n$$

$$F = B_2 (x + iy)^2 + B_6 (x + iy)^6 + B_{10} (x + iy)^{10} + B_{14} (x + iy)^{14} + B_{18} (x + iy)^{18} + \ldots \quad (3.3)$$

where B_2 is the quadrupole gradient. B_n is the potential of the multipole errors in the quadrupole field, which arises in the quadrupole due to a particular pole structure (see the discussions in Section 1.2 of Chapter 1 in particular). It is noted that in the above derivation of Equation 3.3, n=Index of the multipole errors. Since a quadrupole is a fourfold axis-symmetric magnet, only 6,10,14,18, …, n^{th} number of harmonics can be found.

3.4 Good Field Region in a Quadrupole

The good field region of an electromagnet is defined as the horizontal distance from the magnetic center of the magnet, along which the multipole errors are less than the desired number, 0.1% in the case of this thesis. In this thesis, this distance is also called width. As such, the width of the good field region is completely controlled by the multipole errors of an electromagnet, i.e., the higher the multipole errors, the less the width of the good field region. A schematic view of a good field region in a quadrupole is shown in Figure 3.5. For example, in the figure, the blue line shows the good field region of a quadrupole magnet, which needs to be as straight as possible (at least $\pm$1.0 cm from the center in this research) being parallel to X-axis and the Y-axis defines the field error or field quality, which needs to be as low as possible ($\leq$0.1% in this research).

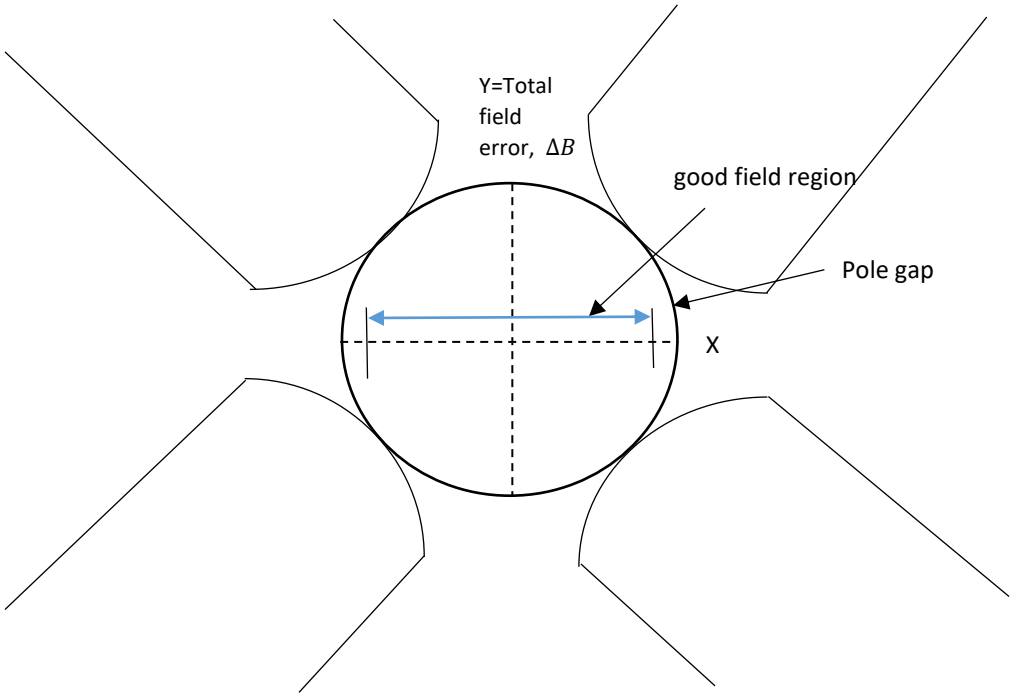

Figure 3.5: An example of Good field region in a quadrupole.

3.5 Governing Equations

The behavior of a magnetic field generated by a quadrupole is govern by the Maxwell's equations. Maxwell's equations are a combination of the equations defining Gauss's law of electricity, Gauss's law of magnetism, Ampere's law and Faraday's law of induction (Hyperphysics.phy-astr.gsu.edu., 2019). Among the four laws, the two are shown in Table 3.1 which are used for magnetostatics simulation of the magnet as this research solved a magnetostatics problem. Magnetostatic problems are the studies where the magnetic field is analyzed due to static electric field. These two laws calculated the behavior of the magnetic field generated from a specific quadrupole including the magnet pole profile and end profile.

Table 3.1: Maxwell's Equations used in the research.

Name	Integral form	Differential form
Gauss's law for magnetism	$\oint \vec{\mathrm{B}} \,.\, \overrightarrow{dA} = 0$	$\vec{\nabla} \,.\, \vec{B} = 0$
Ampere's law	$\oint \vec{\mathrm{B}} \,.\, \overrightarrow{ds} = \mu_0 i + \frac{1}{c^2} \frac{d}{dt} \int \vec{\mathrm{E}} \,.\, \overrightarrow{dA}$	$\vec{\nabla} \times \vec{B} = J$

where

- $\vec{\mathrm{B}}$ = Magnetic flux density (T).
- $\overrightarrow{dA}$ = Area (m^2).
- $\vec{\nabla}$. = Divergence operator.
- $\overrightarrow{ds}$ = Surface (m^2).
- $\vec{\mathrm{E}}$ = Electric flux density (C/m^2).
- $\vec{\nabla} \times$ = Curl operator.
- J = Current density (A/m^2).

Gauss's law for magnetism states that the net magnetic flux is zero within a closed surface around a magnet, i.e. within a closed surface, the number of field lines entering on the surface is equal to the number of field lines leaving from the surface. There is no loss of field lines. In the case of quadrupole, the number of field lines leaving from the North Pole is equal to the number of field lines entering the South Pole within a closed surface. The Ampere's law, which is discussed earlier in this chapter, mainly calculated the magnetic field and its related quantities due to electric currents.

It is noted that the specific governing equation of a magnetic system (e.g., quadrupole) includes the boundary condition, and the equation can only be solved numerically with software. The next section will discuss several well-known software systems for obtaining the behavior of a magnetic field for a particular magnetic system.

3.6 Simulation Software

In designing a magnet for a particular magnet configuration, e.g., quadruple, analytical equations are usually not available. As such, the design is based on simulation, which can be called simulation-based design. In this thesis, three magnetostatic simulation software systems were used to conduct the magnet design. One of them is *POISSON*. POISSON is a two-dimensional magnetic simulation software that is used for optimal design of magnet pole profile for achieving the width of GFR or transversal multiploe errors. This program was developed by Los Alamos Accelerator Code Group (LAACG) (Billen et al., 1993), and is based on a finite element or difference concept specifically the program generates a triangular mesh to fit to the boundaries of different materials of a magnet.

The other two software programs are *RADIA* and *OPERA.* Both of them are a three-dimensional magnetic simulation program that is used to simulate the field along the Z-axis (Figure 1.4) or longitudinal direction. OPERA can do both body mesh and space mesh, while RADIA can only do body mesh. This thesis found that for the optimal design of the end or edge of the magnet, both body mesh and space mesh is needed. As such, this thesis eventually used OPERA for optimal design of the end or edge of the magnet. Further, OPERA was formerly called Vector Fields and was first developed by Rutherford Appleton Laboratory (OperaFEA, 2019). The software treats part of the model that contains the electric field differently to the part of the model without the electric field. As a result, the accuracy of the solution is often far higher than other magnet simulation software.

3.7 Summary

This chapter discussed how to calculate the behavior of the magnetic field generated from a specific electromagnetic system, quadrupole in this case. This behavior includes the multipole error in the field. Therefore, this is a foundation for the optimal design of the geometry of the magnet in a quadrupole, which will be discussed in the next chapter.

Chapter 4 : Optimal Design of the Geometry of Magnet in a Quadrupole

4.1 Introduction

This chapter presents the optimal design of the geometry of the magnet in quadrupole. Optimal design makes sense in that the design problem is formulated as an optimization problem; that is, the decision variable, objective function, and constraint function are defined. However, regarding how the optimization problem is solved, this thesis was limited to a simulation-based trial-and-error procedure, mostly because there is no analytical relation available that links the decision variable to the objective function and constraint function in the context of this research. The simulation software used in this thesis includes POISSON and OPERA which were introduced in Chapter 3. This chapter is organized as follows. Section 4.2 presents the strategy for the optimal design of the magnet as well as the formulation of the optimization problem. Section 4.3 presents the methodology for optimal design of the magnet profile. Section 4.4 presents the result of the optimal design along with some discussions. Section 4.4 is a conclusion. In Appendix D, a preliminary validation of the optimal design is presented, which shows the optimal design is reasonable, but caution should be taken that this validation is not very reliable, and the experimental vilification is warranted in future.

4.2 Strategy and Formulation of an Optimal Design Problem

4.2.1 Design requirement revisiting

First of all, the requirement for the magnet in a quadrupole is put together and revised here below:

(1) The good field region in the x-y coordinate plane should be greater than $\pm 10\ mm$ from the center of the magnet (see Figure 1.6).
(2) Allowable total multipole error is $\leq 0.1\%$ in the good field region.
(3) The field magnetic lines at the edges should be as straight as possible (see Figure 1.7).
(4) The pole width is 1.91 cm (see Figure 1.5).
(5) The pole gap in the quadrupole is 2.4 cm in diameter (see Figure 1.5).

The design of the magnet in this thesis refers to determining the geometry of the magnet, specifically the pole profile in the x-y coordinate plane (see Figure 1.6) and edge profile in the y-z coordinate plane (see Figure 1.7). The pole profile is also called along the **transversal direction** and the edge profile is also called along the **longitudinal direction** (see Figure 4.1). Considering the ease with manufacturing of the magnet, the modified parts on the profile of the existing magnet were decided to be either line or arc in this thesis. It is noted that the profile of the existing magnet is a hyperbola.

4.2.2 Optimal design of the pole profile

Figure 4.2 shows a schematic model for the design of the pole profile. Due to the symmetrical property of the pole profile, only half of the profile was considered. Based on the strategy as discussed before, the design of the pole profile was to modify the profile of the existing magnet, designed by Les Dallin (Dallin, 2018). The optimal design of the pole profile was represented as an optimization problem with the **decision variable** being the modification on the top of the existing pole profile, the **objective function** being the width of the GFR, and the **constraint function** being the multipole error less than 0.1%. Further, there was a constraint that is the modified part of the pole profile must be within the shaded region as indicated in Figure 4.2. The modified part has been named as '**bump**' in this thesis.

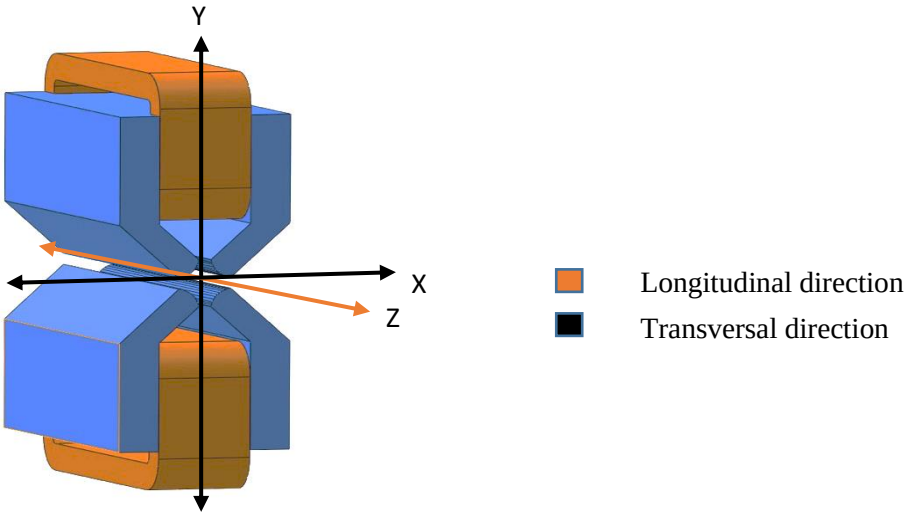

Figure 4.1: Perspective 3D model of the quadrupole showing transversal and longitudinal optimization direction.

In this thesis, a novel idea to represent the bump on the pole profile was proposed. The bump is composed of four points, as shown in Figure 4.3, two of which are on the original profile (a, b), and two points (S1, S2) are in the feasible region for the profile (shaded area in Figure 4.2). Point b is on the corner of the edge and profile, so it cannot be changed. The other three points can be changed to create different bumps or modified parts of the profile. With the foregoing idea, the decision variable or design variable is the three points (a, S1, S2). Accordingly, the constraint function with regard to these three points becomes (1) Point a can only be changed along the original profile, and (2) S1 and S2 must be in the feasible region for the profile (the shaded areas in Figure 4.2). The objective function remains the same as stated before.

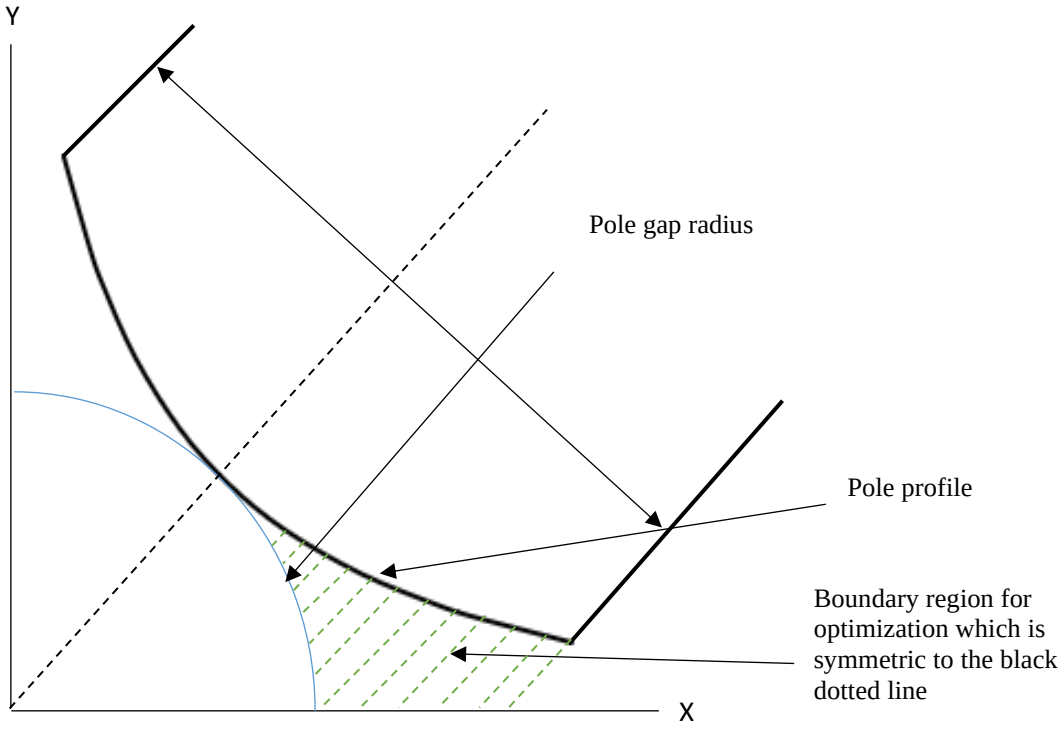

Figure 4.2: Boundary region for optimization has been shown with the green dotted lines. Both sides of the black dotted line are symmetric. Constraints that were followed while optimization; fixed pole width and pole gap.

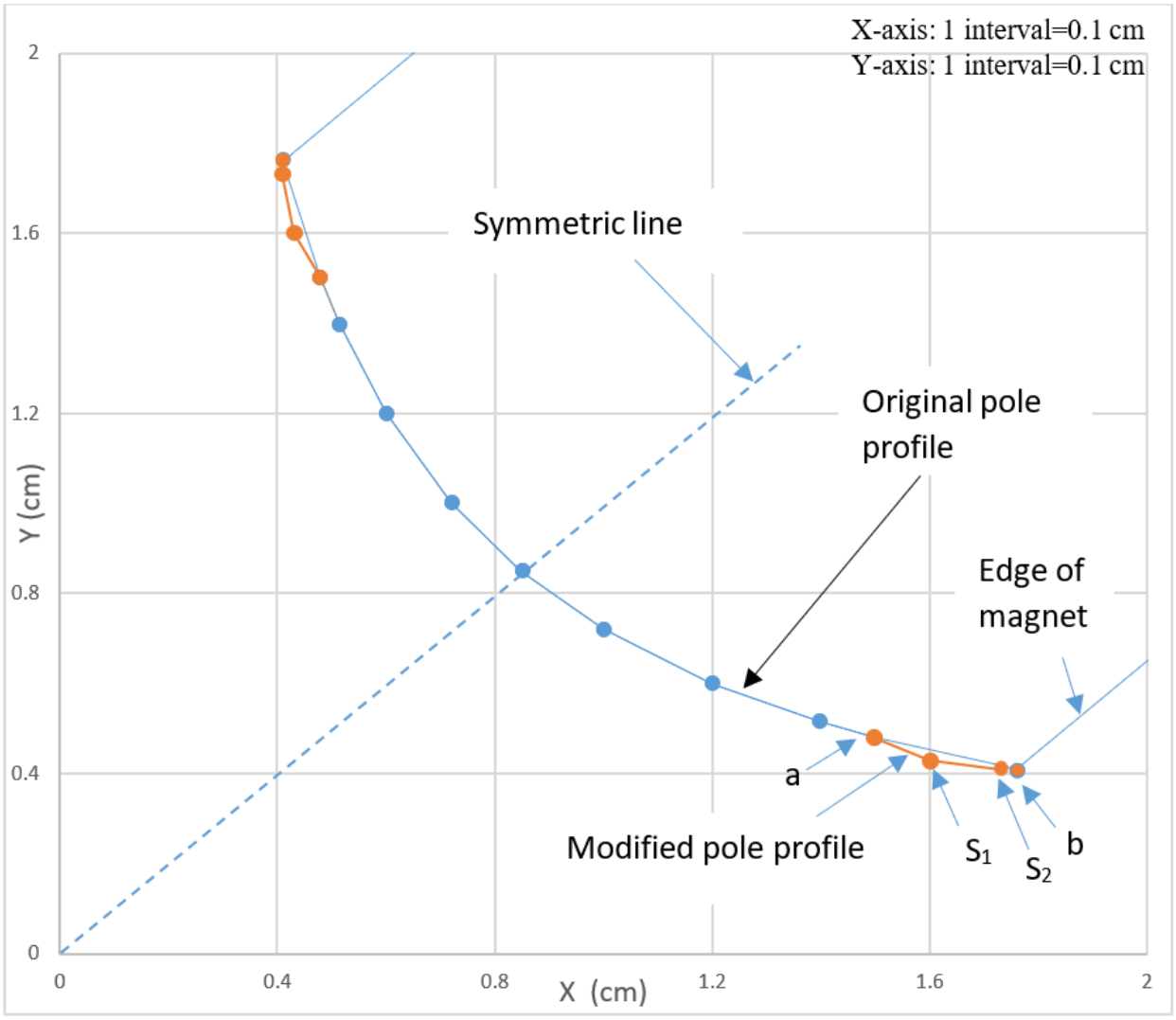

Figure 4.3: Pole profile modification (the modified part is called bump).

The algorithm to change a, S1, and S2 and to find the best of them, say a*, S1*, S2* was a trial-and-error procedure, as there is no analytical solution available for the multipole errors but a numerical solution via the software POISSON (discussed in Chapter 3). This algorithm (Algorithm I) is shown below.

Algorithm I (for optimal design of the pole profile):

(1) **INITIAL CREATION** of a, S1, S2; {a must be on the existing profile}

Flag_a=0; {Flag: the variable representing the status of whether a is updated}

Flag_S1=0; {Flag: the variable representing the status of whether S1 is updated}

Flag_S2=0; {Flag: the variable representing the status of whether S2 is updated}

(2) **RUN** POISSON to get the amplitude of the harmonics (error) and the width of GFR (W_GFR);

IF (Flag_a=1) **THEN** Flag_a=0;

IF (Flag_S1=1) **THEN** Flag_S1=0;

IF (Flag_S2=1) **THEN** Flag_S2=0;

(3) **IF** (W_GFR < 10 cm) **OR** (W_GFR is not large enough) **THEN**

IF Flag_a=0 **THEN** (update a; Flag_a=1; GO TO (2))

IF Flag_S1=0 **THEN** (update S1; Flag_S1=1; GO TO (2))

IF Flag_S2=0 **THEN** (update S2; Flag_S2=1; GO TO (2))

(4) **END**

Remark 1: In the above algorithm, the update operation was performed by the user, which is subjective and empirical. In Appendix E, one can find the update on a, S1, and S2, respectively; the change step is 0.01 to both x-coordinate and y-coordinate.

Remark 2: The whole algorithm was run by the user, which is manual. For instance, the (3) was evaluated by the user, the judgment on "sufficient large" in particular.

4.2.3 Optimal design of the edge profile

The sharp corner of the magnet (see Figure 4.3, Point b) is responsible for the curved field line and large amplitude of the multipole error or harmonics (see Figure 1.7). Therefore, the edge side of the magnet needs to be modified such that the field line can be as straight as possible and the amplitude of the harmonics on the field line can be as small as possible. Based on the strategy, that is, the profile being easy for manufacturing, the modified edge took the straight face, as illustrated in Figure 4.4. In this thesis, a more quantitative analysis of the straightness of the field line was

not attempted in the modified design of the magnet edge side, but any modification which can increase the corner angle from 90 degrees to a larger one will be conducive to the straightness of the edge side. Therefore, this thesis considered determining the edge modification to reduce the amplitude of the harmonics on the field line only.

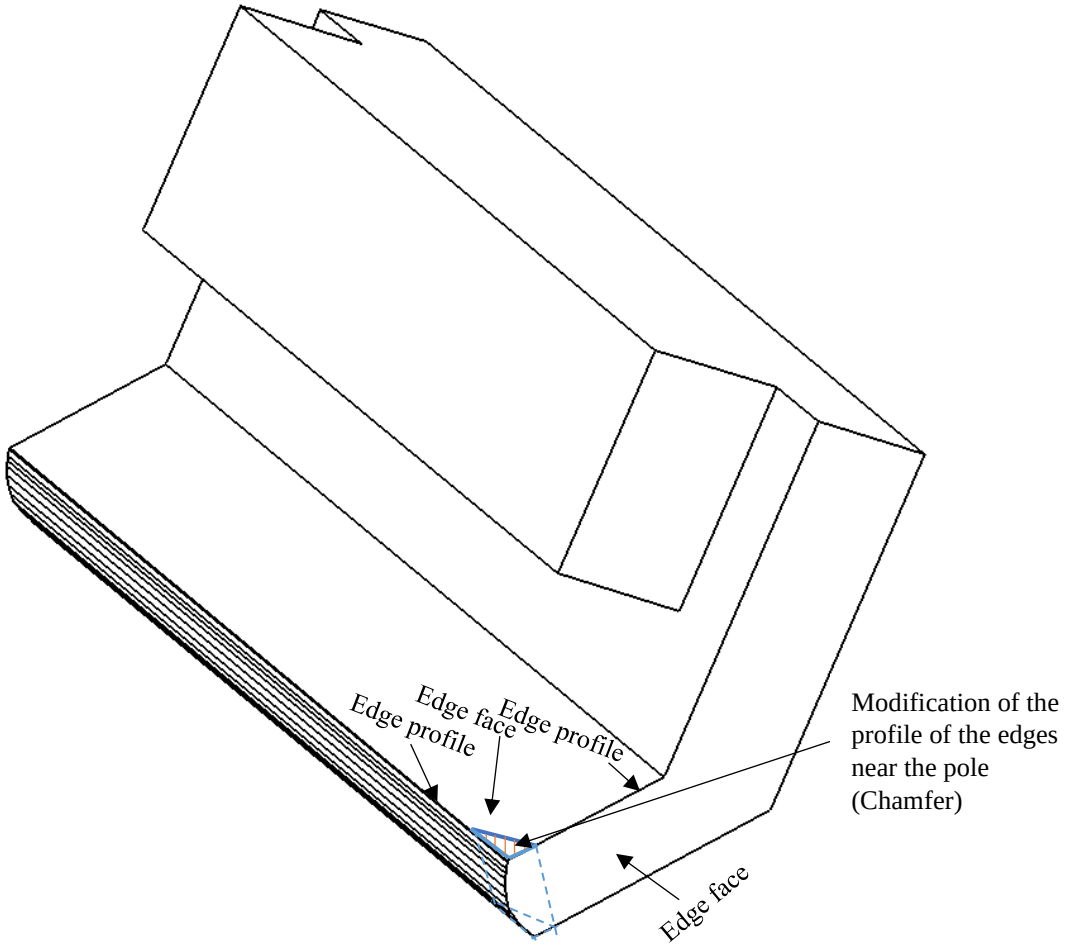

Figure 4.4: Magnet yoke in three-dimensional space. A chamfer is created by removing material from the edge of each magnet pole.

The modified design problem can be formulated as an optimization problem, in which the objective function is the amplitude of the harmonics of the field line on the modified edge, the constraint function is that the modified profile or face needs to be within the original shape of the magnet, and the decision variable or optimal variable is the edge profile or face (see Figure 4.4). This edge

face is further represented by two points ‘a’ and ‘b’, as illustrated in Figure 4.5b, and that is to say, Point a and Point b will change along the lines where they stay (Figure 4.5b). The optimal design was to determine the location of a and b, respectively, so that the objective function gets a minimum.

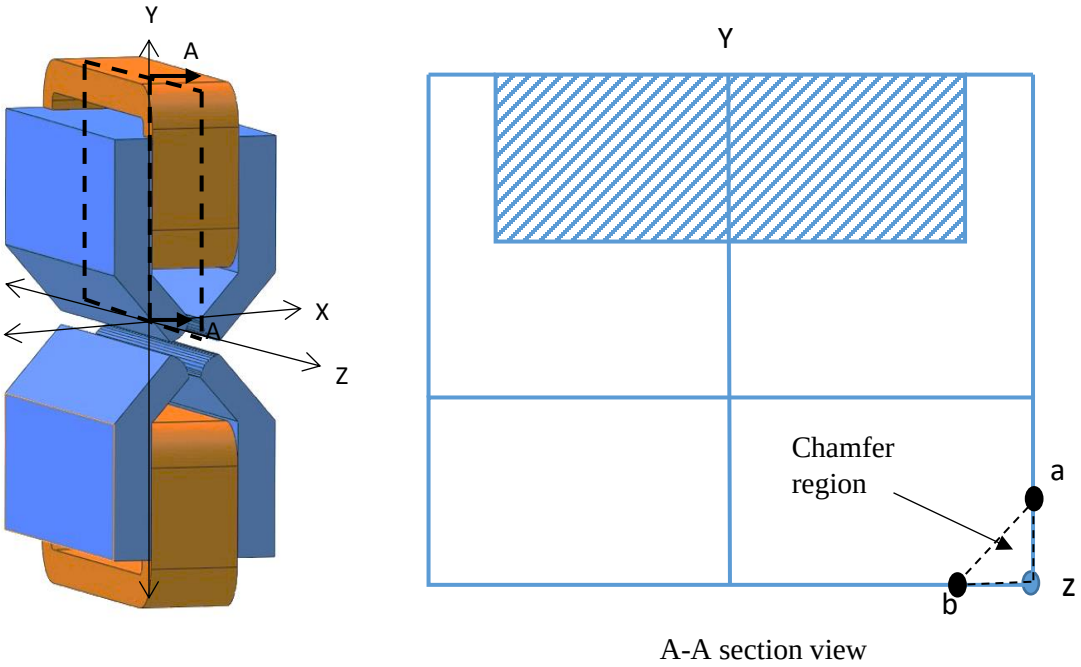

Figure 4.5: (a) Perspective 3D model of the magnet indicating the section A-A, (b) Section view of A-A showing the points a and b that move on the edge line and create a chamfer region.

Again, because there is no analytical solution available to the relation between the modified edge and the harmonics on the field line, a simulation software package OPERA (see the discussion in Chapter 3) was employed, which can calculate the harmonics given the modified edge, harmonics from 3 to 8 in particular. The algorithm to determine Point a and Point b was a trial-and-error procedure, which is shown below (Algorithm II):

Algorithm II (for optimal design of the edge profile):

(1) INITIAL CREATION of a, b; {a, b must be on the existing edge of the magnet}

Flag_a=0; {Flag: the variable representing the status of whether a is updated}

Flag_b=0; {Flag: the variable representing the status of whether b is updated}

(2) **RUN** OPERA to get the amplitude of the harmonics (error);

IF (Flag_a=1) **THEN** Flag_a=0;

IF (Flag_b=1) **THEN** Flag_b=0;

(3) **IF** (error is greater than 0.1%) **OR** (error is not small enough) **THEN**

IF Flag_a=0 **THEN** (update a; Flag_a=1; GO TO (2))

IF Flag_b=0 **THEN** (update b; Flag_b=1; GO TO (2))

(4) **END**

Remark 3: In the above algorithm, the update operation was performed by the user, which is subjective and empirical. In Appendix F, one can find the update on a, b, respectively; the change step is 0.5 to both z-coordinate and y-coordinate.

Remark 4: The whole algorithm was run by the user, which is manual. For instance, the (3) was evaluated by the user, the judgment on "not small enough" in particular.

4.3 Results and Discussions

4.3.1 The result of the optimal design of the magnet pole profile

Figure 4.6a shows the modified pole profile of the magnet, and Figure 4.6b shows the harmonics on this profile. The profile of Figure 4.6a is with the 1:1 scale to the real system. Figure 4.7 compares the existing pole profile and the modified pole profile. Figure 4.8 shows the GFR for the exiting pole profile and the modified pole profile. From this figure it can be seen that the width of the GFR of the modified pole profile is significantly wide than that of the existing pole profile; the width of the GFR of the modified pole profile is nearly ±1.1 cm. Table 4.1 shows the comparison of the harmonics of the field for the existing pole profile and the modified pole profile. It can be seen from this table that the amplitudes of harmonics are reduced to the most harmonics except B_2. The quadrupole gradient B_2 has increased due to some geometry adjustment on the top part of the yoke (Top part of the yoke was lengthened 1 cm in the existing model along Y-axis). It is noted that this adjustment on the top part of the yoke has no impact on the other harmonics except quadrupole gradient. Figure 4.9 gives the similar information to that of Table 4.1.

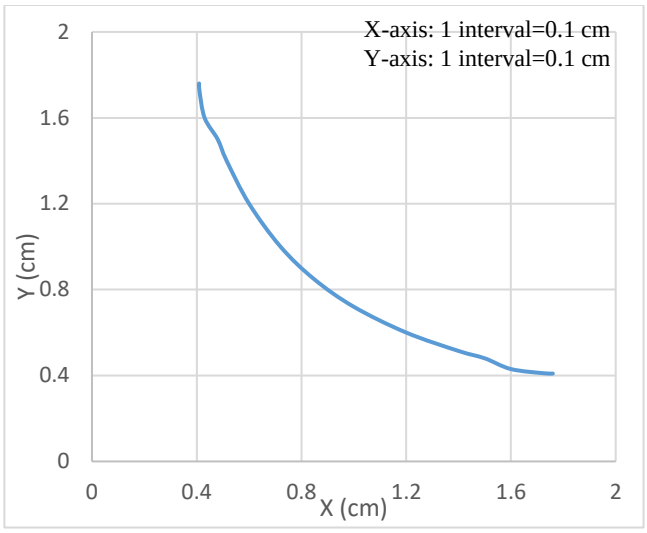

2	5.5809E+03
6	-3.3077E-01
10	8.2867E-01
14	-8.9632E-01
18	4.6123E-03
22	1.9432E-01
26	3.9019E-01

(a) (b)

Figure 4.6: (a) Optimized pole shape, (b) Optimized harmonic values (Field coefficient of the harmonics are in Gauss and distance is in cm).

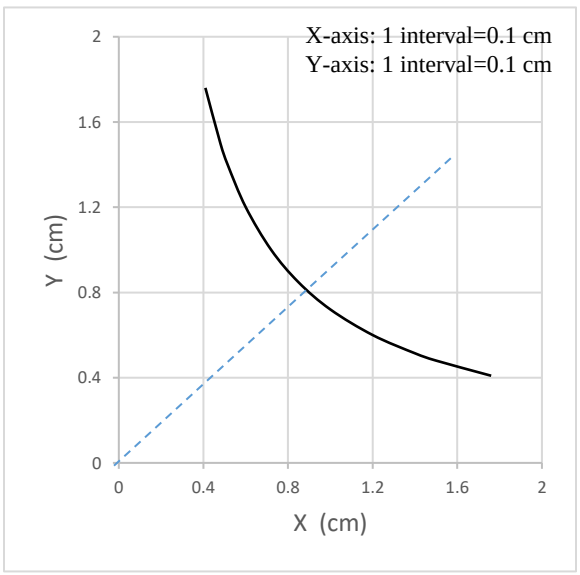

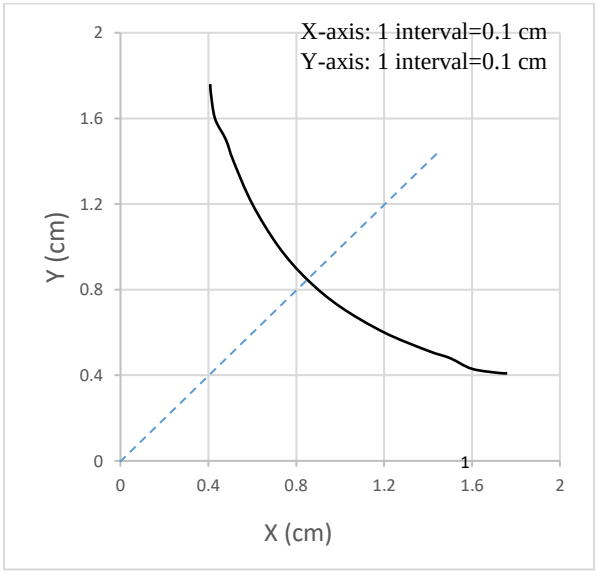

(a) (b)

Figure 4.7: Comparison of the pole profile: (a) the existing one, (b) the modified one.

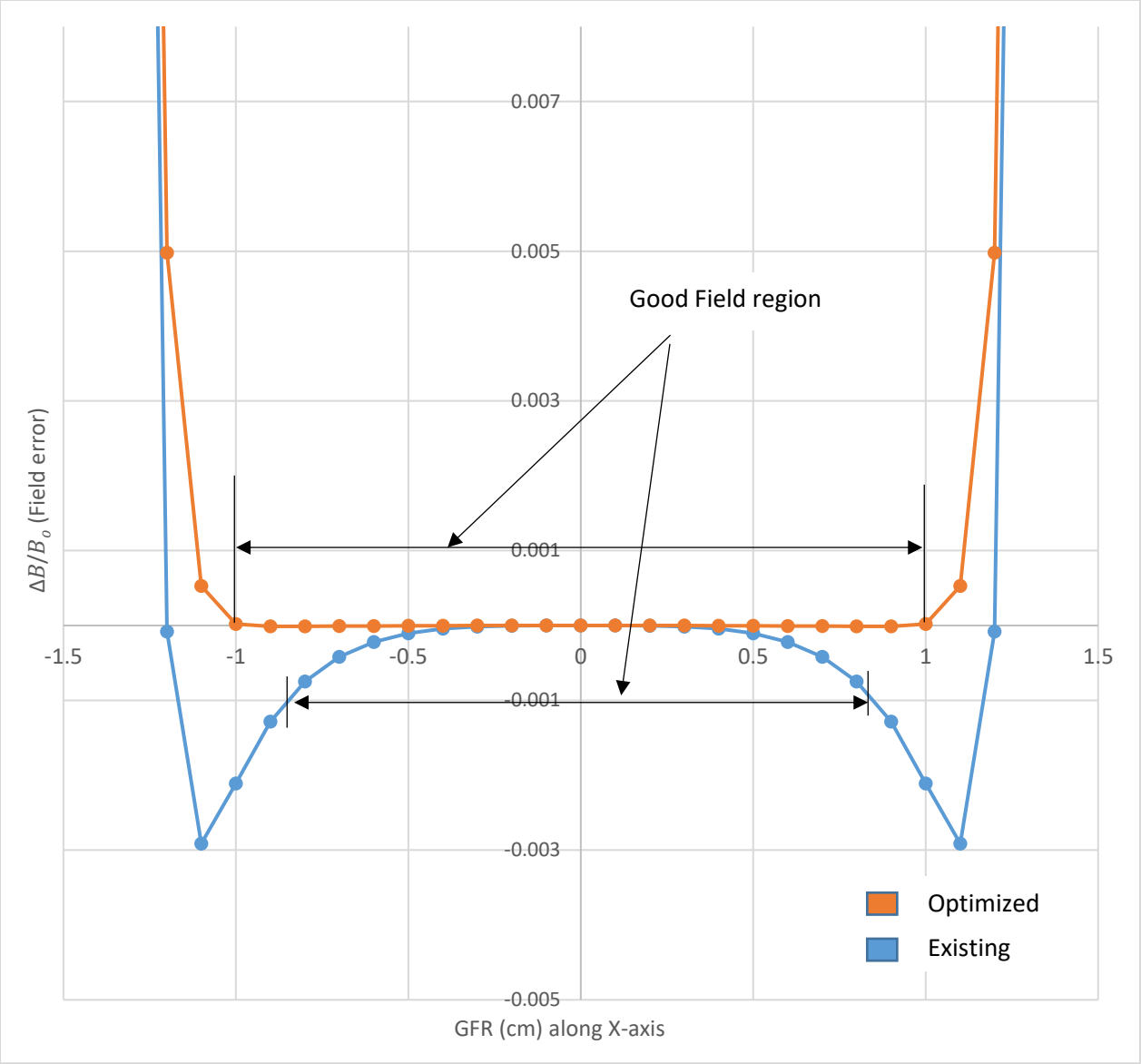

Figure 4.8: Comparison of the GFR for the existing pole profile and the modified pole profile

Table 4.1: Amplitude of the multipole errors of the existing pole profile and the modified pole profile after the optimal design (on a circle of radius 1.0 cm inside the pole gap). Field coefficient of the multipole errors are in Gauss (G) and distance is in cm.

Multipole error	**Existing Pole profile**	**Modified pole profile**	**Percentage Change (%)**
B_2	5406	5580	+3.21
B_6	-8.8408	-0.33077	-96.26
B_{10}	-2.0988	0.82867	-139.483
B_{14}	-1.0726	-0.89632	-16.43
B_{18}	0.06497	0.004612	-92.90
B_{22}	0.19474	0.19432	-0.21
B_{26}	0.35001	0.31919	-8.80546

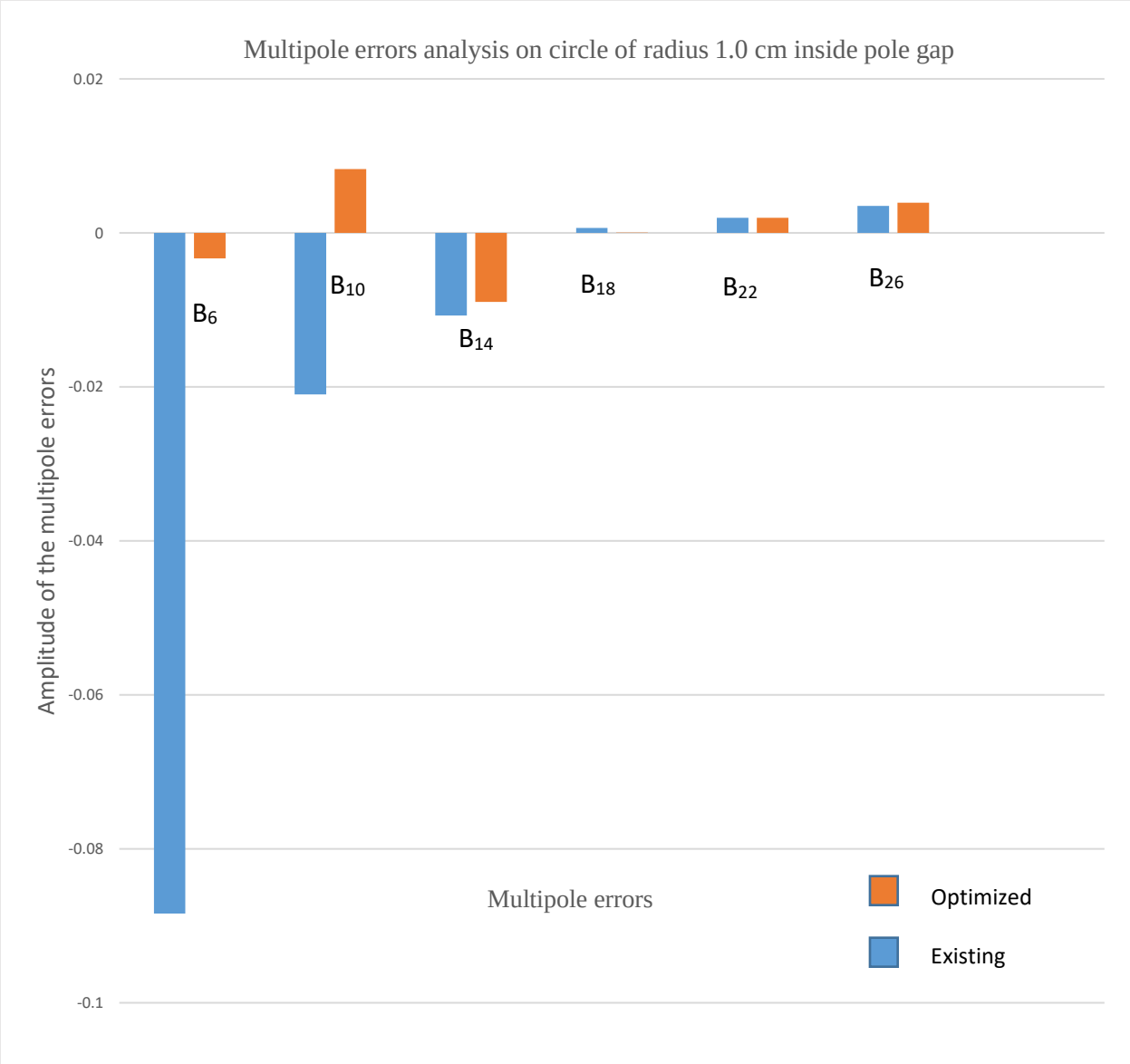

Figure 4.9: Amplitude of the multipole errors of the existing and modified pole profile.

4.3.2 The result of the optimal design of the magnet edge profile

Figure 4.10 shows both the existing edge profile and the modified edge profile in the 1:1 scale to the real system. Figure 4.11 illustrates the modified edge of the magnet in 3D to give a more vivid impression of the modified edge. Table 4.2 shows the comparison of the harmonics of the field for the exiting edge profile and the modified edge profile. It can be seen from this table that the

amplitudes of harmonics are reduced with the modified edge, and to the modified edge profile, all but B_9 (about 0.2%) are less than or near to 0.1%. Figure 4.12 gives the similar information to that of Table 4.2. Figure 4.13 shows the field along the z-axis or longitudinal direction for the modified edge profile of the magnet. It can be seen from this figure that the field does not change with respect to the existing edge profile of the magnet, which means that the modified edge has no impact on the field distribution of the magnet along the Z-axis.

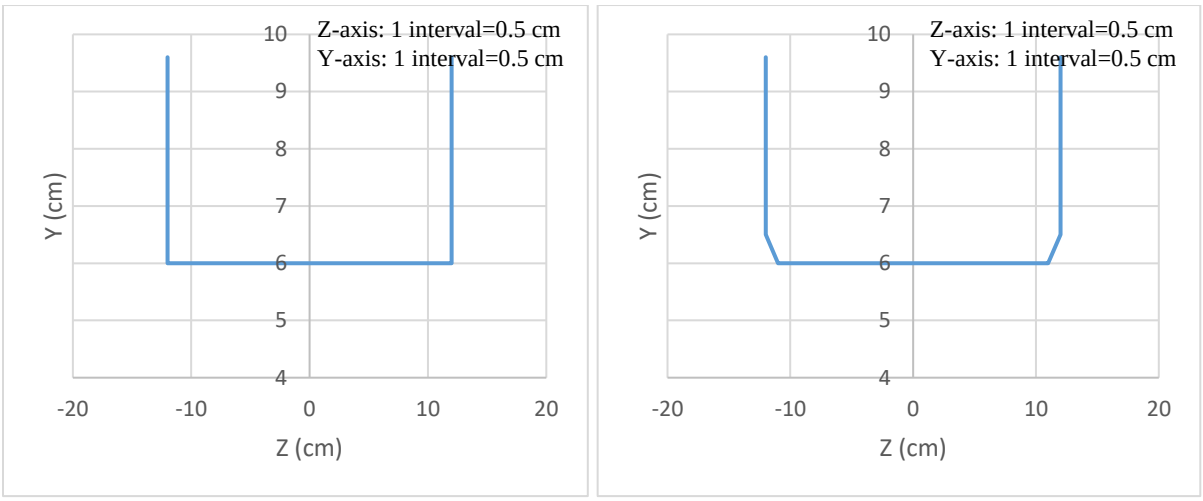

(a) (b)

Figure 4.10: (a) Existing edge profile, (b) modified edge profile.

(a) (b)

Figure 4.11: Edge pole profile of (a) existing, (b) optimized model

Table 4.2: Amplitude of the multipole errors of the existing edge profile and the modified edge profile (on a circle of radius 1.0 cm at the edge of the magnet). Field coefficient of the multipole errors are in Gauss (G) and distance is in cm.

Multipole error	**Existing model**	**Optimized model**	**Percentage change (%)**
B_3	4.08	1.71	-58.08
B_4	-2.17	-14.80	582.028
B_5	1.44	-0.384	-126.667
B_6	-67.8	-26.60	-60.767
B_7	-1.44	-7.64	430.556
B_8	-3.94	0.302	-107.665
B_9	-8.00	-26.70	233.75
B_{10}	6.32	6.27	-0.791
B_{11}	2.86	-9.060	-416.783
B_{12}	-1.03	12.20	-1284.47
B_{13}	-2.40	-10.60	341.667
B_{14}	0.927	1.17	26.2136
B_{15}	-1.79	8.10	-552.514
B_{16}	-1.34	1.44	-207.463
B_{17}	-1.77	0.223	-112.599
B_{18}	1.87	14.10	654.011

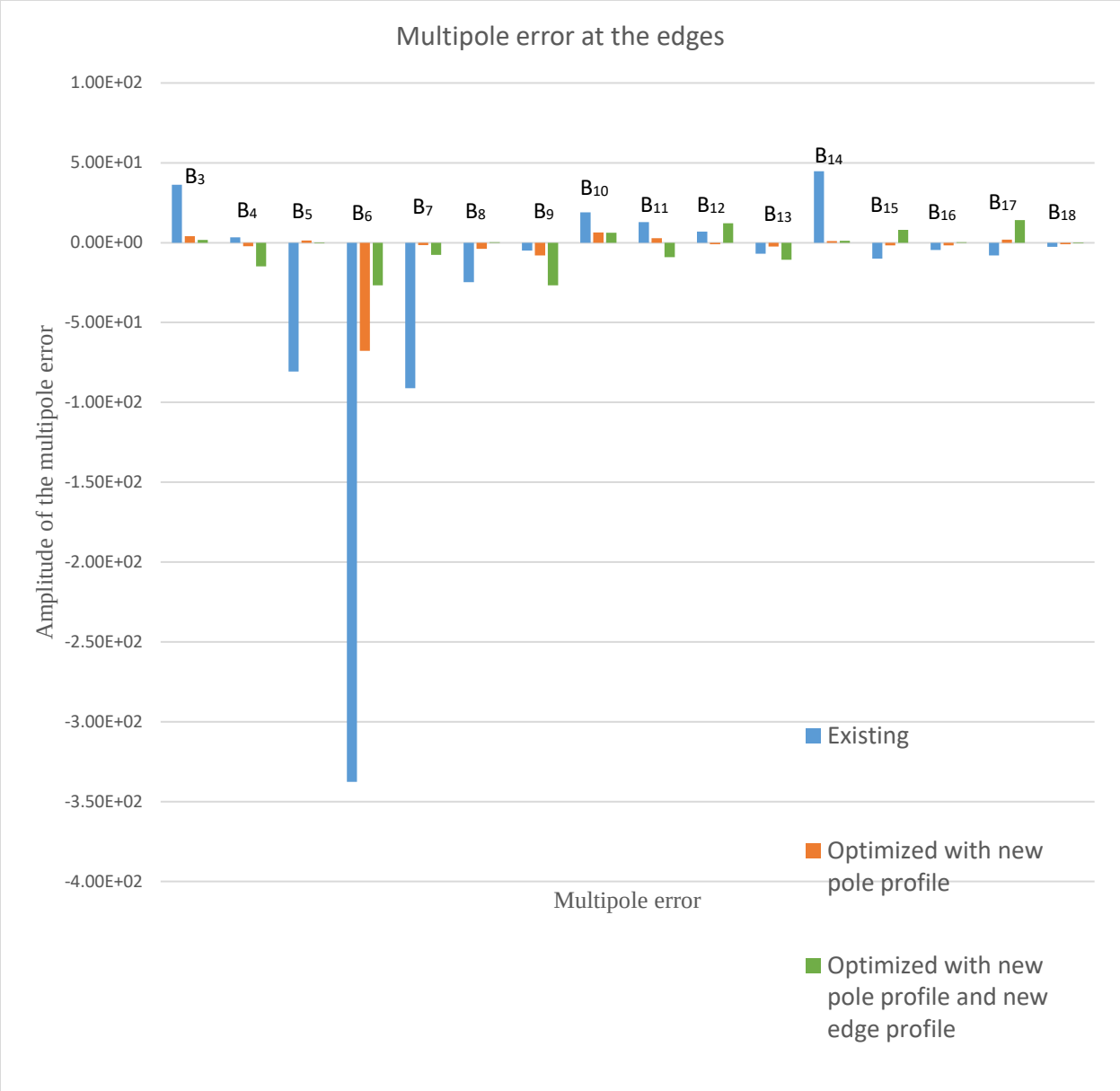

Figure 4.12: Amplitude of multipole errors at the edge of the magnet.

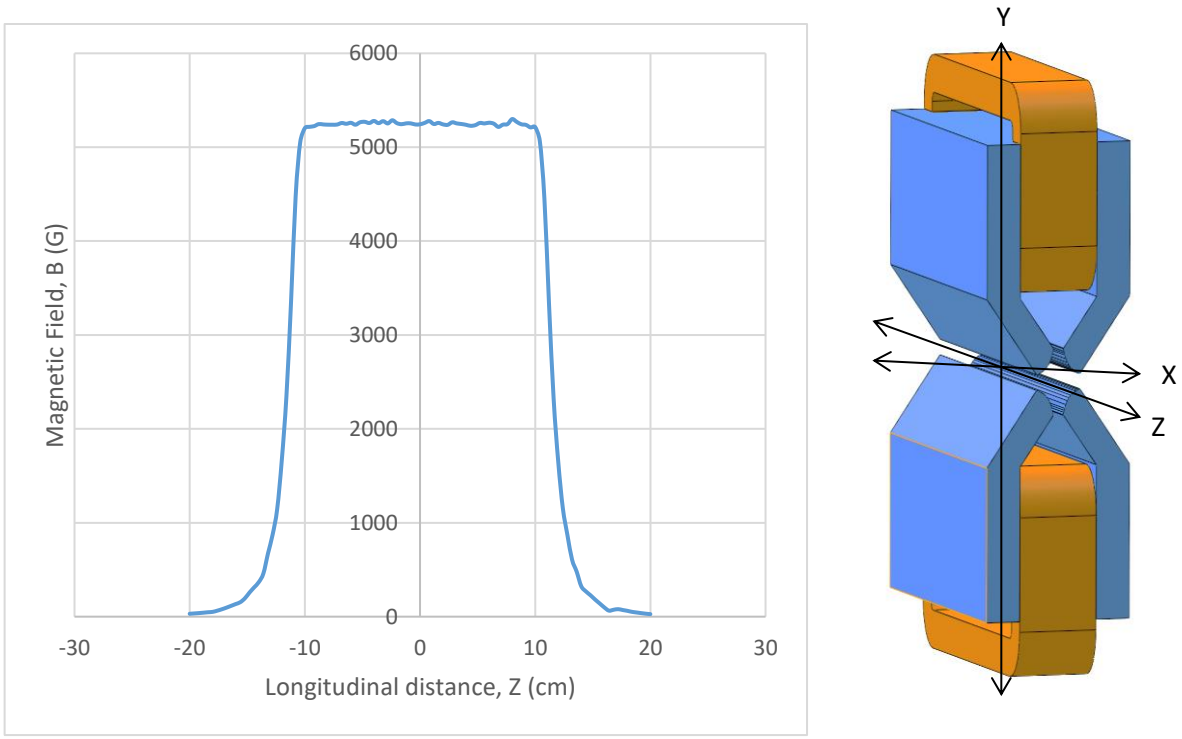

Figure 4.13: (a) Field distribution along the Z-axis, at an X=1.0 cm offset, (b) perspective model of the quadrupole to show the direction of field distribution.

4.4 Summary and Conclusions

A new idea for the optimal design of the magnet, the profile in both the transversal direction and the longitudinal direction, was presented in this chapter. The new idea is to modify the existing profile (hyperbole) by a set of straight-line segments in light of easy manufacturing of the magnet. The optimal design makes sense to the determination of the specification of these line segments. The quality of the field is characterized by (1) the width of the GFR along the transversal direction (the x-axis), (2) the amplitude of the harmonics in the field region, including the magnet profile, (3) the amplitude of the harmonics of the field along the longitudinal direction (the z-axis), and (4) the quadrupole gradient. The simulation-based trial-and-error optimization procedure was applied to conduct the modified design.

It can be concluded from the result obtained that (i) the width of the GFR was 2.2 cm ($\pm$1.1 cm) within the total multipole error 0.1% as opposed to 1.6 cm (±0.8 cm) of the existing design, (ii) the field line is more straight, and (iii) the efficiency of the field remains to be similar.

Chapter 5 : Conclusions and Recommendation

5.1 Overview and Conclusions

The overall objective of this thesis research was to improve the design of the magnet in a quadrupole at CLS, as opposed to the existing design which is available at CLS. The existing design does not meet the requirement, which includes: (i) the width of the good field region (GFR) should be larger than ±1.0 cm (the multipole error is less than 0.1%), and (ii) the field line surrounding the edge should be as straight as possible with the multipole error on the edge as small as possible (e.g., less than 0.1%). The new design was expected to meet the foregoing requirement.

The design includes (1) the pole profile design and (2) the edge profile design. There were two specific objectives for this overall objective, namely

- ***Objective 1****: To propose a new design concept for the profile of the pole of a quadrupole magnet so as to increase the width of GFR to be as much as possible (at least greater than* ±1.0 cm from the center of the magnetic field).

- ***Objective 2:*** *To propose a new design concept to the magnet, especially the profile of the edge of the magnet so that the bad edge effect with the magnet can be reduced.*

The new design concept has two points. The first point is that the modified profile (both the pole profile and the side profile) is composed of straight line, which is the geometry easiest for manufacturing. The second point is that the design problem was formulated into an optimization problem to make the design improvement exercise more rational.

Chapter 2 presented a literature review, especially the work on the modified design of the magnet in literature. The review further confirmed the need of the proposed research. In Chapter 3, the foundation for analyzing the magnetic field given the magnet was presented; especially two simulation systems for the magnetic field, POISSON and OPERA, were presented, which are the

tools that were relied upon to conduct design improvement in this thesis. The optimal design for the pole profile and edge profile was presented in Chapter 4 with a great success.

The following conclusions can be drawn from the results presented in Chapter 4:

(1) The new design concept, using straight line to form modified profile of the magnet in the pole profile as well as the edge profile, is effective to the quadrupole system, and significantly improves the existing magnet design at CLS.

(2) The modified pole profile can achieve the width of GFR with ±1.1 cm (> ±1.0 cm as required), as opposed to the ±0.8 cm of the existing magnet design, referring to Objective 1 of this research.

(3) The modified edge profile can achieve the amplitude of the harmonics on the edge profile with less than 0.1%, referring to Objective 2 of this research.

It is noted that the magnet concerned in this thesis is the one with the recessed coils (Figure 1.2a).

5.2 Limitations

There were some limitations with this work. The first limitation is related to the mesh size with the software OPERA for the design of the edge of the magnet. Currently, the mesh size is 0.05 cm, and smaller ones were hindered to run because of the restriction of the computer memory. Another limitation with the software OPERA is that it was not capable of calculating the field line, so the quantitative measure of the straightness of the magnetic field line on the edge was not available to guide the optimal design of the edge of the magnet.

5.3 Future Works

There are several future works derived from this thesis. First, in this thesis, the good field region was the region where the multipole error is less than 0.1% but the multipole error was calculated in the x-y coordinate plane at the center of the magnet. However, in fact, this multipole error may not capture the 3D nature of the field. In future, a 3D measure may be proposed and used to guide the optimal design of the magnet pole profile. Second, in this thesis, for the pole profile, only two line segments with two points on the original profile (i.e., a, b) were used to form the modified profile. More generally, first there may be more than two line segments, second, Point b may not

be the corner point, and finally the selection of Point a on the original profile may be such that the line connecting a and S1 is tangential to the original profile at Point a, so as to make the modified profile smoother. It is noted that a smoother profile is favored in terms of the quality of the field, reduced multipole errors.

5.4 Contribution

This thesis has made a contribution in the field of magnet design in general and magnet design for a quadrupole magnetic system in particular. The design in particular makes sense to the pole profile design (in the x-y coordinate plane or transversal design) and to the side profile design (in the y-z coordinate plane or longitudinal design). The idea proposed in this thesis is such that the modified profile is composed of several straight-line segments on the top of the existing curve. The manufacturing of the proposed profile of the magnet is thus very easy, as it does additional manufacturing (i.e., manufacturing on the modified part) on the straight-line segment only. This idea has never been tried in the literature for designing the magnet in any magnetic system.

References

Billen, J. H., Young M. L., (1993) “POISSON/SUPERFISH on PC Compatibles,” in Proc. PAC’93, Washington DC, USA.

Chubar, O., Elleaume, P., Chavanne, J. (1998) “A 3D Magnetostatics Computer Code for Insertion Devices,” J. Synchrotron Rad. vol. 5, no. 19, pp 481-484.

Dallin, L.O., Bertwistle, D., (2018) “Magnet Design Considerations for an Ultralow Emittance Canadian Light Source” 9th International Particle Accelerator Conference (IPAC2018), Vancouver, BC, Canada.

Elleaume, P., Chubar, O., Chavanne, J., (1997) “Computing 3D Magnetic Field from Insertion Devices,” in Proc. PAC’97. Vancouver, Canada.

Holmes, J., Henderson, S., Zhang, Y., (2009) “Magnetic Fields, and Magnet Design”.

Hyperphysics.phy-astr.gsu.edu. (2019). HyperPhysics. [Online] Available at: http://hyperphysics.phy-astr.gsu.edu/hbase/hframe.html [Accessed 30 Jul. 2019].

Kalimov, A., Potienko, A., Wollnik, H. (2006). Optimization of the Pole Shape of Quadrupole Magnets by MULTIMAG. IEEE Transactions on Applied Superconductivity, 16(2), pp.1282-1285.

Le Bec, G., Chavanne, J., N’gotta, P., m (2014) “Shape Optimization for the ESRF II Magnets” 5th International Particle Accelerator Conference, IPAC2014, Dresden, Germany.

Merzouki, R., Samantaray, A. K., Pathak, P. M., (2012). Intelligent Mechatronic Systems: Modeling, Control, and Diagnosis. Springer Science & Business Media. pp. 403–405. ISBN 978-1447146285.

Nocedal, J., Wright, S., (1999). Numerical optimization. New York: Springer. ISBN 0-387-98793-2

OperaFEA. (2019). Magnetostatics. [Online] Available at https://operafea.com/product/solutions-modules/magnetostatics/ [Accessed 30 Jul. 2019].

Opentextbc, ca., (2019). Magnetic Fields Produced by Currents: Ampere's Law – College Physics. [online] Available at: https://opentextbc.ca/physicstestbook2/chapter/magnetic-fields-produced-by-currents-amperes-law/ [Accessed 5 Oct. 2019].

Tani, N., Watanabe, Y., Hotchi, H., Takayanagi, T., Togashi, T., Horino, K. (2016). Optimization of the Pole Shape for Corrector Quadrupole Magnet in the J-PARC 3-GeV RCS. IEEE Transactions on Applied Superconductivity, 26(4), pp.1-4.

Tanabe, J., (2005) "Iron Dominated Electromagnets, Design, Fabrication, Assembly and Measurements".

Zickler, T., (2009) "Basic design and engineering of normal-conducting, iron-dominated electromagnets" CERN Accelerator School.

Appendix A: Dimensions of the quadrupole

Figure A.1 shows the dimensions of the existing quadrupole magnet. (All dimensions are in mm.)

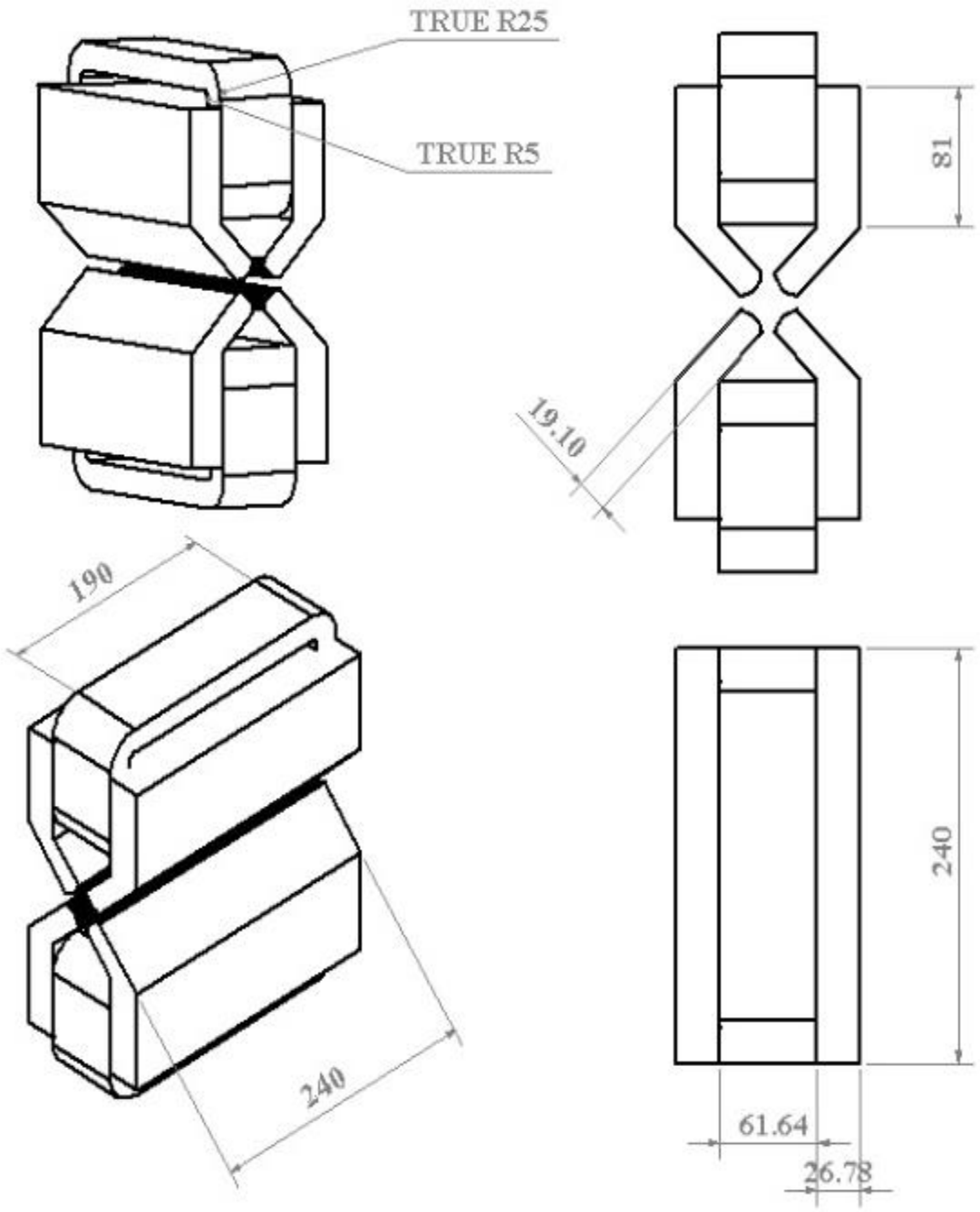

Figure A.1: The dimensions of the existing magnet.

Appendix B: Software code for the optimized pole profile.

This section provides POISSON code for the modified pole profile of one quadrant of the whole magnet.

```
QUAD (compact)
Field output is requested along the X-axis
[Originally appeared in 1987 Reference Manual B.2.1]

; Copyright 1987, by the University of California.
; Unauthorized commercial use is prohibited.

&reg kprob=0,          ; Declares a POISSON problem
dx=.05,                ; Mesh interval
mode=0                 ; Using internal table for material 2
IENERGY=1
conv=1.
xminf=-0,xmaxf=3.0183,       ; X range for field interpolation
yminf=0,ymaxf=0,       ; Y range (along line y = 0)


; The next 6 terms refer to the harmonic analysis:
ktype=4,               ; quad symmetry
nbslf=1.
nterm=5,               ; Number of coefficients
nptc=14,               ; Number of arc points for interpolation
rint=1.,           ; Radius of the arc
angle=90,              ; Angular extent of arc (default start = 0)
rhogam=.0005,
rnorm=1.&              ; Aperture radius

&po x=0.0,y=0.0 &
&po x=10.,y=0. &
&po x=10.,y=16. &
&po x=0.,y=16. &
&po x=0.0,y=0.0 &

&reg mat=3, mtid=3 &  ; TR quadrant
&po x=5.76,y=4.4091 &
&po x=1.76,y=.4091 &
&po x=1.73,y=.41 &
&po x=1.6,y=.43 &
&po x=1.5,y=.48 &
&po x=1.4,y=.51429 &
&po x= 1.2,y=.6 &
&po x=1.,y=.72 &
```

```
&po x=.84853,y=.84853 &
&po y=1.,x=.72 &
&po y= 1.2,x=.6 &
&po y=1.4,x=.51429 &
&po y=1.5,x=.48 &
&po y=1.6,x=.43 &
&po y=1.73,x=.41 &
&po y=1.76,x=.4091 &
&po x=3.0582,y=4.4091 &
&po x=5.76 ,y=4.4091 &

&reg mat=3, mtid=3 &
&po x=5.76,y=4.4091 &
&po x=3.082 ,y=4.4091 &
&po x=3.082 ,y=11.4041 &
&po x=5.76,y=11.4041 &
&po x=5.76,y=4.4091 &

&reg mat=3, mtid=3 &
&po x=0 ,y=7.4041 &
&po x=3.082 ,y=7.4041 &
&po x=3.082 ,y=11.4041 &
&po x=0,y=11.4041 &
&po x=0 ,y=7.4041 &

&reg mat=1, cur=-4020 & ; coil
&po x=0,y=4.4091 &
&po x=3.,y=4.4091 &
&po x=3.,y=6.4091 &
&po x=0.,y=6.4091 &
&po x=0,y=4.4091 &

&reg mat=1, cur=4020 & ; coil
&po x=0.,y=12.4091 &
&po x=3.,y=12.4091 &
&po x=3.,y=14.4091 &
&po x=0.,y=14.4091 &
&po x=0.,y=12.4091 &

&mt mtid=3
bgam=0.00000E+00 0.0000000
2003    0.00149755
3204    0.001248401
4004.5 0.00112374
5005.5 0.001098851
5606    0.001070361
```

7908 0.001011602
9310 0.001074148
11014 0.001271127
12016 0.001331517
13020 0.001536051
14028 0.001996036
15240 0.002624673
16260 0.00369
16980 0.004711427
17300 0.005780313
18700 0.010695191
19900 0.02010051
20400 0.029411775
20700 0.038647357
20950 0.047732714
22000 0.090909123
24000 0.166666726 &

Appendix C: 3D simulation with OPERA

The 3D simulation was run to reduce edge errors. The simulation was performed on the whole magnet body where each simulation took on an average of 1.5 days to run. This running time of the simulation basically depends on the determination of the boundary volume, mesh size and computer configuration. The mesh size that has been used for the final 3D simulation was 0.05 cm for the whole body and the boundary up to which the magnetic field distribution calculated was a cylinder of 12 cm radius and 30 cm long.

Appendix D: Validation

Verification and validation are a very important part of a design to make it reliable. Most of the design processes use simulation software for design purposes. The result from the software needs to be properly checked to validate the design. One of the ways to check the validity of the design is to check the design analytically. In this research, the optimization of the pole shape has been performed using two software systems to meet the determined objectives. To check the validity of the magnetic model, the result from the software has been checked analytically.

A point of cartesian coordinate (x=0.84853cm, y=0.84853cm, z=0cm) has been selected on the pole profile (see Figure D.1). The quadrupole field for that particular point has been figured out analytically first and then from the software, OPERA.

Field at a point (Analytical process) (All dimensions are in cm).

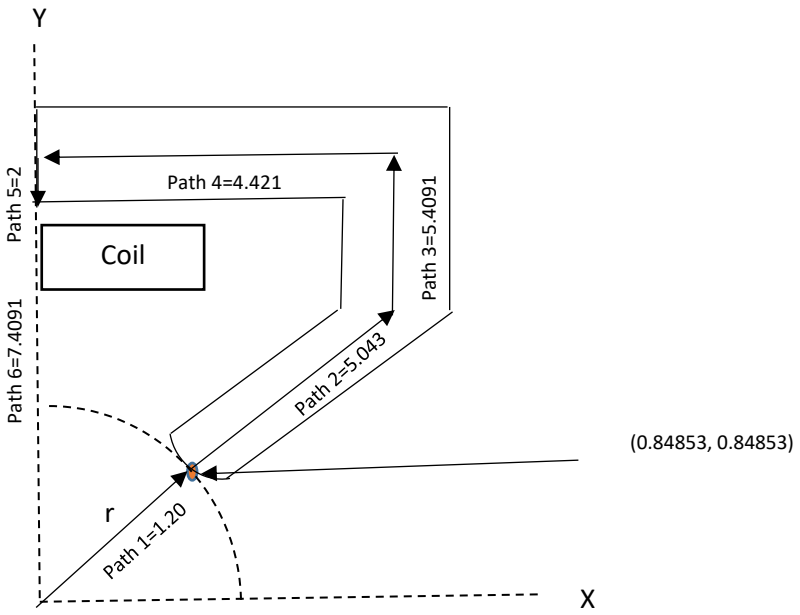

Figure D.1: Quadrupole excitation. Checking the validity of the model.

The total magnetic field along the magnetic circuit (Path 1+path 2+ path 3+ path 4 + path 5+ path 6) is,

$$\oint \frac{\vec{B}}{\mu\mu_0}\overrightarrow{dl} = \oint \frac{\vec{B}}{\mu_0}\overrightarrow{dl} + \oint \frac{\vec{B}}{\mu\mu_0}\overrightarrow{dl} + \oint \frac{\vec{B}}{\mu\mu_0}\overrightarrow{dl} + \oint \frac{\vec{B}}{\mu\mu_0}\overrightarrow{dl} + \oint \frac{\vec{B}}{\mu\mu_0}\overrightarrow{dl} + \oint \frac{\vec{B}}{\mu_0}\overrightarrow{dl}$$

$$\oint \frac{\vec{B}}{\mu\mu_0}\overrightarrow{dl} = \underset{\text{Path 1}}{\oint}\frac{\vec{B}}{\mu_0}\overrightarrow{dl} + \underset{\text{Path 2}}{\oint}\frac{\vec{B}}{\mu\mu_0}\overrightarrow{dl} + \underset{\text{Path 3}}{\oint}\frac{\vec{B}}{\mu\mu_0}\overrightarrow{dl} + \underset{\text{Path 4}}{\oint}\frac{\vec{B}}{\mu\mu_0}\overrightarrow{dl} + \underset{\text{Path 5}}{\oint}\frac{\vec{B}}{\mu\mu_0}\overrightarrow{dl} + \underset{\text{Path 6}}{\oint}\frac{\vec{B}}{\mu_0}\overrightarrow{dl}$$

……. (D.1)

For quadrupole the gradient, B' is constant. So, the magnetic field, B= $' \times l$.

For low carbon steel, AISI 1010, $\mu \geq 100$ Henry/m; $\mu =$ Magnetic permeability of steel.

From Equation (4.5), $\oint \frac{\vec{B}}{\mu\mu_0}\overrightarrow{dl} = \int_0^{r=1.2}\frac{B'\times r}{\mu_0}dl + \underset{\text{Path 2}}{\oint}\frac{B\times 5.043}{\mu\mu_0}\overrightarrow{dl} + \underset{\text{Path 3}}{\oint}\frac{B'\times 5.4091}{\mu\mu_0}\overrightarrow{dl} + \underset{\text{Path 4}}{\oint}\frac{B'\times 4.421}{\mu\mu_0}\overrightarrow{dl} + \underset{\text{Path 5}}{\oint}\frac{B\prime\times 2}{\mu\mu_0}\overrightarrow{dl} + \underset{\text{Path 6}}{\oint}\frac{B\prime\times 7.4091}{\mu_0}\overrightarrow{dl}$

$= \int_0^{r=1.2}\frac{B\prime\times r}{\mu_0}dl + \oint\frac{B\prime\times 4.2r}{\mu\mu_0}\overrightarrow{dl} + \oint\frac{B\prime\times 4.5r}{\mu\mu_0}\overrightarrow{dl} + \oint\frac{B\prime\times 3.6r}{\mu\mu_0}\overrightarrow{dl} + \oint\frac{B\prime\times 1.67r}{\mu\mu_0}\overrightarrow{dl} + \oint\frac{B\prime\times 6.17r}{\mu_0}\overrightarrow{dl}$

$= \frac{B\prime r^2}{2\mu_0} + \frac{4.2\,B\prime r^2}{100\times 2\mu_0} + \frac{4.5\,B\prime r^2}{100\times 2\mu_0} + \frac{3.6\,B\prime r^2}{100\times 2\mu_0} + \frac{1.67\,B\prime r^2}{100\times 2\mu_0} + \frac{6.17\,B\prime r^2}{100\times 2\mu_0}$

$= \frac{B\prime r^2}{2\mu_0}(1 + \frac{4.2+4.5+3.6+1.67+6.17}{100})$

$= \frac{B\prime r^2}{2\mu_0}$ (1.20) ……..……. (D.2)

NI is the total amount of current supplied to the coil to generate the quadrupole gradient, $\acute{B}$ in Equation 4.6.

According to Maxwell inhomogeneous equation, (Tanabe, 2005)

$$\oint \frac{\vec{B}}{\mu\mu_0}\overrightarrow{dl} = \frac{B'r^2}{2\eta\mu_0} = NI$$

NI= $\frac{B\prime r^2}{2\eta\mu_0}$ ……. (D.3)

where,

NI= Total current= number of turns in coil × current

= 48 turns × 83 Amp

= 4020 Amp-turns.

B'= Quadrupole gradient (T/cm).

μ_0= permeability in air (N/A^2).

η= Magnet efficiency= $\frac{NI_{gap}}{NI_{gap}+NI_{yoke}}$ ……..……...(D.4)

The total length of the path on the yoke is = (5.043+5.4091+4.421) =14.8731cm and the permeability of steel yoke is 100 times of permeability of air. From Equation 4.8,

η= $\frac{NI_{gap}}{NI_{gap}+NI_{gap}\times\frac{14.8731/1.2}{100}}$ =0.90= 90%.

Now putting all the values in Equation 4.6 for a particular point on the pole profile, (x= 0.84853cm, Y= 0.84853cm), quadrupole field found for that point is,

NI= $\frac{B\prime r^2}{2\eta\mu_0}\times 1.20$

4020 = $\frac{B\prime(1.2)^2}{2\times0.90\times1.257\times10^{-6}}\times 1.2$

B'= 0.5264 T/cm= 5264 G/cm

So, the magnetic field for that point is, B= $B'\times r$= 5264 × 1.2

= 6316 G

Field at a point (in OPERA)

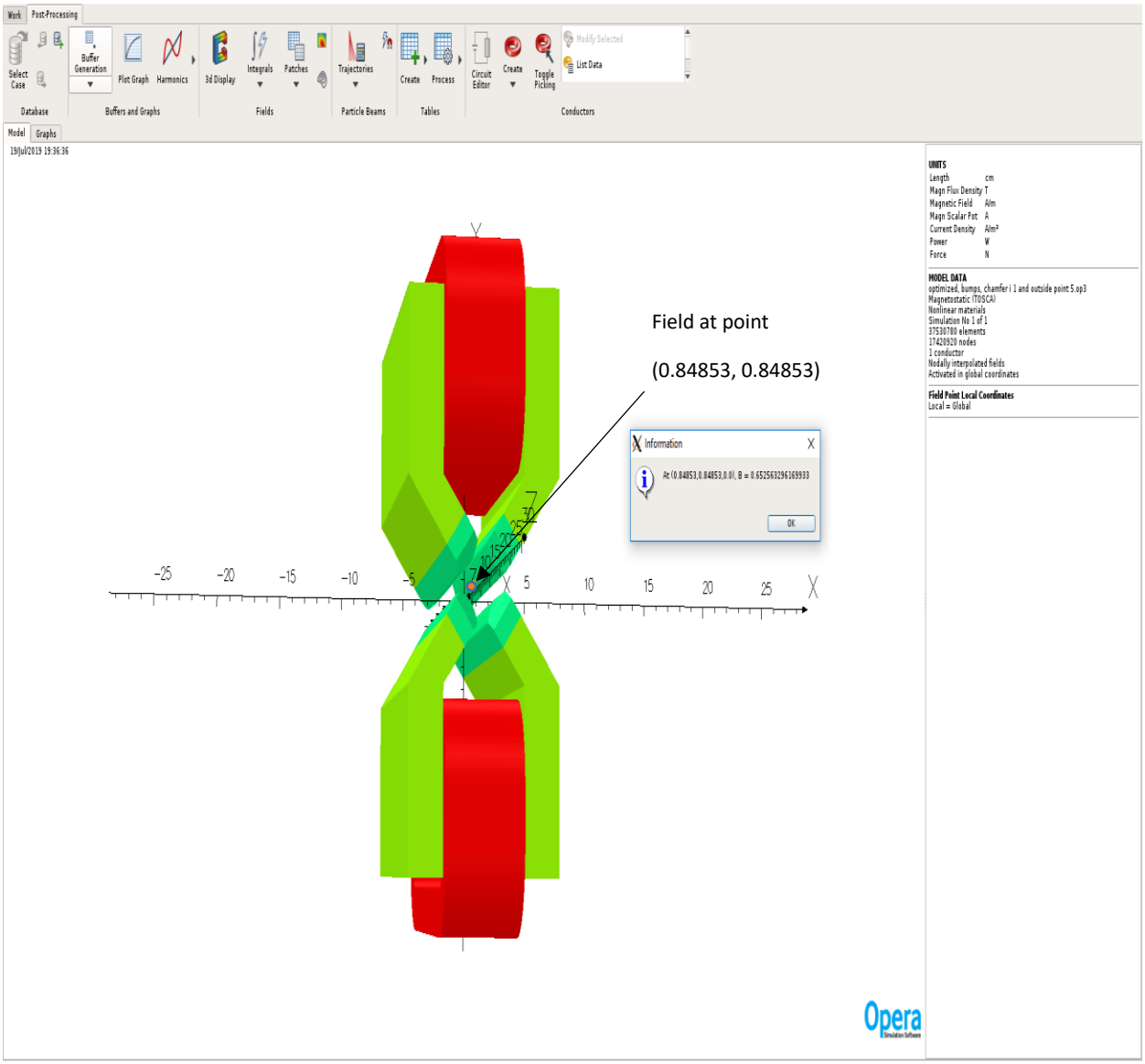

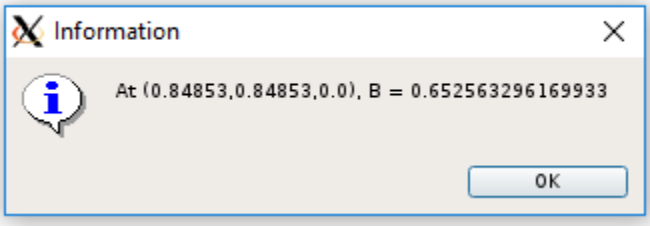

The analytical value of the field for that particular point is 6315 G and from the simulation, it was found 6525 G which is very close. The reason for a little greater value from the simulation is because of the mesh size. Adjustment of different mesh sizes gives very little different value of the field but still, are pretty close to the analytic value (see Table D.1) which justifies the generated code for the pole shape as quite authentic.

Table D.1: Field at a point (x=0.84853cm, y=0.84853cm, z=0cm)

Mesh Size (cm)	**Field (G) from simulations**	**Analytic value of the filed (G)**
0.045	6525	
0.065	6383	6316
0.080	6233	

Appendix E: Coordinates of the Points for the trial for Bump

In this section, the coordinates of the points a, S_1, S_2, which were used for the trials to find the final bump shape on the profile are given (Table E.1). All the coordinates are in cm on the XY plane.

Table E.1: The trial coordinates for a, S1, S2 in the optimal design of the pole profile

a (x, y)	S_1 (x, y)	S_2 (x, y)
1.65, 0.40	1.67, 0.44	1.755, 0.39
1.63, 0.42	1.67,0.44	1.755, 0.39
1.63, 0.42	1.66, 0.45	1.755, 0.39
1.63, 0.42	1.66, 0.45	1.75, 0.40
1.61, 0.44	1.66, 0.45	1.75,0.40
1.61, 0.44	1.65,0.46	1.75, 0.40
1.61, 0.44	1.65, 0.46	1.745,0.40
1.60, 0.45	1.65, 0.46	1.745, 0.40
1.60, 0.45	1.64, 0.47	1.745, 0.40
1.60, 0.45	1.64, 0.47	1.740, 0. 39
1.58,0.47	1.64, 0.47	1.740, 0.39
1.58, 0.47	1.635,0.46	1.740, 0.39
1.58, 0.47	1.635, 0.46	1.735, 0.40
1.56, 0.47	1.635, 0.46	1.735, 0.40

1.56, 0.47	1.625, 0.46	1.735, 0.40
1.56, 0.47	1.625, 0.46	1.732, 0.40
1.535, 0.47	1.625, 0.46	1.732, 0.40
1.535, 0.47	1.62, 0.44	1.732, 0.40
1.535, 0.47	1.62,0.44	1.73, 0.41
1.50, 0.48	1.62, 0.44	1.73, 0.41
1.50, 0.48	1.60, 0.43	1.73, 0.41

Appendix F: Coordinates of the Points for the trial for Chamfer

Table F.1 shows the trials of the two points b, a, in the optimal design of the edge profile. All the coordinates are in cm on the YZ plane.

Table F.1: Trial coordinates of the points b, a.

b (z, y)	a (z, y)
11.0, 0.0	0.0, 1.0
11.5, 0.0	0.0, 1.0
11.5, 0.0	0.5, 0.0
11.0, 0.0	0.0, 0.5